Distinct Regulaton of Bioenergetics and Translation by Gp I mGluRs and NMDARs

Sudhriti Ghosh Dastidar[1,2], Sumita Chakraborty[1], Sumantra Chatterji[1,3], Aditi Bhattacharya[1], Ravi S Muddashetty[1,4,*]

[1]Institute for Stem Cell Biology and Regenerative Medicine, Bangalore, India

[2]Manipal Academy of Higher Education, Manipal, India

[3]National Center for Biological Sciences, Bangalore, India

[4] Lead Contact

* Correspondence: ravism@instem.res.in

Abstract

Neuronal actvity is majorly responsible for dispropotionally large consumption of energy by the brain. However little is known about the nature of the processes responsible for abundant ATP outlay within neurons. Here we provide evidence that major fraction of ATP consumed on glutamate stimulation in cultured cortical neurons is due to activation of global *de-novo* protein synthesis mediated by group I mGluRs. On the contrary NMDAR stimulation leads to a much slower yet protein synthesis dependant ATP expenditure. We found mGluR and NMDAR stimulation impacting the kinetics of translation with distinct kinetics; while mGluR lead to rapid and sustained translation activation as measured by eEF2 phophorylation and matabolic labeling, NMDAR stimulation induced an intial translation inhibition followed by a delayed activation. Translation kinetics for these receptors were always found to have an inverse correlation with Neuronal ATP consumtption. Interestingly, we identified that AMP activated protein kinase (AMPK) has a central role in regulating downstream effects of both mGluR and NMDAR. AMPK activity was reduced on mGluR stimulation even under low ATP levels while there was a rapid increase in AMPK actvity on NMDAR stimulation. Perturbing AMPK function prior to either stimulation led to a complete loss of stimulation specific effects on eEF2 phosphorylation and global translation. Our observation therefore established a pivotal role for AMPK-eEF2 signaling axis on receptor specific regulation of global translation.

43 **Introduction**

44 Brain is known to consume a significant fraction of the body's metabolic energy even
45 at the 'resting' state [1] which increases further on actvity. Evidences from FMRI based
46 studies and PET studies with various tracer molecules have established direct
47 correlations between brain activity and enhanced resource consumption. Conditions
48 such as hypoglycemia and cerebral ischemia leads to severe consequences largely due
49 to perturbations in energy supply [23]. Dysregulated energy metabolism is at the heart of
50 conditions such as epilepsy and various neuro-degenerative diseases [45]. Therefore,
51 highly regulated energy management is a key requirement for proper cognitive
52 functions of the brain.

53 Synapses are thought to be the sites of major ATP consumption [67] due to large number
54 of cellular processes being activated on arrival of a stimulus. While high rate of
55 endocytosis is reported to consume maximum energy at the pre-synaptic boutons on
56 electrical stimulation [89], our understanding is quite limited as to what extent various
57 processes consume ATP at the post-synaptic compartments and at the pan-neuronal
58 level. Neuronal activity has also been known to induce abundant protein synthesis [10], a
59 determining resource for long term synaptic plasticity and memory formation. Since
60 each round of amino acid incorporation requires 4 ATP molecules along with additional
61 ATP required for amino acid charging and initiation [1110], any change therefore in the
62 rate of global protein synthesis is expected to have a reflection on the steady state ATP
63 level. Group I metabotropic glutamate receptors (mGluRs referred hereafter) and
64 NMDARs are widely implicated to facilitate or induce various forms of syanptic plasticity
65 across different brain regions [1213]. While mGluRs are known to activate translation

66 rapidly [14][15], NMDAR stimulation causes translation inhibition at an immediate time scale
67 [16]. Considering the distinct nature of their downstrem regualtion, it would therefore be
68 interesting to understand the impact of mGluR and NMDAR activation on cellular
69 energetics.

70 Neuronal activity is also known to trigger ATP production through activation of
71 glycolysis and oxidative phosphorylation [8][17][18][19] to support the enhanced consumption.
72 One key molecular player in such a scenario would be AMP activated protein kinase
73 (AMPK). AMPK is a known sensor for cellular ATP/AMP ratio and acts to balance various
74 catabolic and anabolic processes including global translation [20]. AMPK activation has
75 been shown to be critical to support synaptic ATP level on neuronal activity [17] and
76 influence various forms synaptic plasticity [21][22]. Thus, understanding how AMPK
77 coordinates activity dependent changes on energetics and translation is of paramount
78 importance. To gain deeper insight at the molecular level of regulation of energy
79 metabolism and translation on neuronal activity, we addressed the following questions:
80 1) How is the energy level altered over time on synaptic activity 2) What are the
81 machanisms that play a key role to dynamically regulate translation on various different
82 stimulations and 3) How AMPK activity is altered to strike a balance between energy
83 and translation regulation.

84 Here we report that stimulation with glutamate, the major neurotransmitter in
85 vertebrate CNS, causes large amount of energy consumption primarily due to the
86 activation of global translation by mGluRs at post synapse and globally throughout the
87 neuron. We also report a distinct difference in the kinetics of translation regulation
88 induced by mGluRs and NMDARs. These distinct responses in turn depend on the

89 differential activation of AMPK downstream of mGluRs and NMDARs involving
90 mechanisms mutually exclusive. Finally, we show that acute prior perturbations of
91 AMPK function lead to complete loss of translation regulation on both stimulations
92 thereby establishing AMPK as biochemical coupling mechanism between energetics and
93 translation on neuronal activity.

94 **Results:**

95 **mGluR dependent protein synthesis consumes significant amount of neuronal ATP**
96 **following glutamate stimulation:**

97 To assess the impact of translation on global ATP levels, we used cultured cortical
98 neurons from Sprague Dawley (SD) rats and stimulated with glutamate (25μM) for 5
99 minutes at day *in vitro* 15 (DIV 15) in presence or absence of protein synthesis inhibitors
100 anisomycin or cycloheximide. We then quantified the ATP/(ATP+ADP) ratio from cell
101 lysates using bioluminescence-based methods (**Figure 1A**). Glutamate Stimulation alone
102 led to significant reduction in the neuronal ATP/(ATP+ADP) ratio. This reduction in the
103 ratio was found to be absent on stimulation in presence of protein synthesis inhibitors
104 anisomycin (25μM) or cycloheximide (100μg/ml) (**Figure 1B**) while drugs alone had no
105 significnat impact. The identical effects of both anisomycin and cycloheximide negates
106 the possibility of off-target effects of these drugs. Thus our observations suggest a large
107 increase in protein synthesis on stimulation, responsible for consuming signifcant
108 fraction of neuronal ATP.

109 Further, to understand the contributions from individual glutamate receptors, we
110 repeated glutamate stimulation inhibiting either ionotropic NMDA and AMPA receptors

111 with a cocktail of D-AP5 (25μM) + CNQX (40μM) (refered to as inotropic glutamate
112 receptor (iGluR) blocker cocktail hereafter) or inhibiting mGluRs with MPEP (10μM). Co-
113 stimulation with iGluR blocker cocktail led to significant reduction in ATP/(ATP+ADP)
114 ratio similar to glutamate alone while stimulation along with MPEP abolished the
115 glutamate mediated reduction significantly (**Figure 1C**). Therefore, these results
116 suggest that the observed reduction in ATP on glutamate stimulation is majorly due to
117 mGluR activity with minimal contributions from the iGluRs. Furthermore, Stimulation
118 in presence iGluR blocker cocktail along with protein synthesis inhibitor anisomycin
119 removed the energy burden significantly (**Figure 1B**) corroborating a robust increase in
120 protein synthesis in absence of iGluR activity consumes significant fraction of neuronal
121 ATP. To further investigate on this idea, we stimulated cortical neurons with mGluR
122 and NMDAR specific agonists s-3,5 DHPG and NMDA (agonists of mGluR and NMDAR
123 respectively). While DHPG treatment led to a significant reduction in ATP/ATP+ADP
124 (79.5±3.8%), NMDA had no significant impact **(Supplementary figure 1A)** ascertaining
125 the importance of mGluR activity on energy consumption. To account for the
126 contribution from endocytosis on glutamate mediated ATP consumption, we blocked
127 GTP dependent enzyme dynamin with small molecule inhibitor dynasore (100μM).
128 Stimulation in presence dynasore had similar effects as that of glutamate alone
129 (**Supplementary figure 1B)** suggesting activity induced vesicle endocytosis has
130 negligible effect on pan-neuronal ATP level.

131 To understand the impact of mGluR and NMDAR stimulation on synaptic energy level,
132 we prepared synaptoneurosomes from whole rat cortices at post-natal day 30 (P30) and
133 stimulated with DHPG (100μM) and NMDA (50μM) respectively (**Figure 1D**).

134 Synaptoneurosome preparation was validated with enrichment of synaptic marker PSD
135 95 without any significant enrichment of glial marker GFAP (**Figure 1E**). Synaptic ATP
136 levels showed significant reduction on mGluR stimulation (**Figure 1F**). The reduction in
137 synaptic ATP levels on stimulation was abolished in presence of mGluR inhibitor MPEP,
138 protein synthesis inhibitor anisomycin and cycloheximide (**Figure 1F**) indicating
139 changes in synaptic ATP level on mGluR stimulation is majorly due to protein synthesis.
140 NMDAR stimulation on the contrary had no significant effect on synaptic ATP level and
141 was unaltered in presence of NMDAR inhibitor D-AP5 (**Figure 1F, supplementary figure**
142 **1C**). Therefore, our observations suggest mGluR dependent protein synthesis creates
143 significant energy demand both at the synaptic and pan-neuronal level.

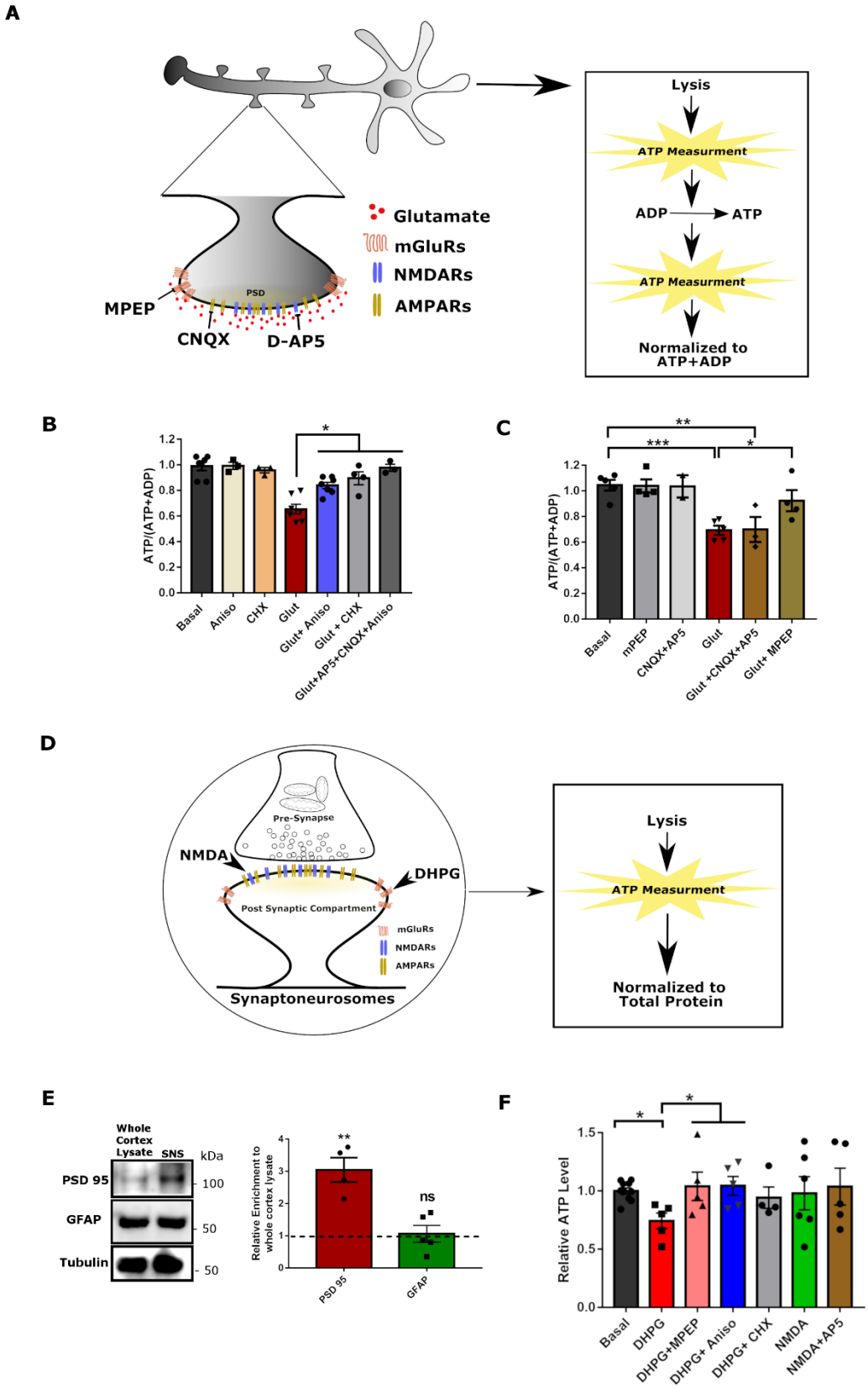
A
Glutamate
mGluRs
NMDARs
AMPARs
PSD
MPEP
CNQX
D-AP5
Lysis
ATP Measurment
ADP
ATP
ATP Measurment
Normalized to ATP+ADP
B
ATP/(ATP+ADP)
Basal
Aniso
CHX
Glut
Glut+ Aniso
Glut + CHX
Glut+AP5+CNQX+Aniso
C
ATP/(ATP+ADP)
Basal
mPEP
CNQX+AP5
Glut
Glut +CNQX+AP5
Glut+ MPEP
D
Pre-Synapse
NMDA
DHPG
Post Synaptic Compartment
mGluRs
NMDARs
AMPARs
Synaptoneurosomes
Lysis
ATP Measurment
Normalized to Total Protein
E
Whole Cortex Lysate
SNS
kDa
PSD 95
GFAP
Tubulin
Relative Enrichment to whole cortex lysate
ns
PSD 95
GFAP
F
Relative ATP Level
Basal
DHPG
DHPG+MPEP
DHPG+ Aniso
DHPG+ CHX
NMDA
NMDA+AP5

145 **Legend for Figure 1**

146 **Glutamate dependent changes in neuronal ATP/ADP Ratio is primarily due to Group I mGluR**
147 **dependent protein synthesis.**

148 **(A)** Schematic depicting experimental work flow for measurement of ATP/ATP+ADP ratio from
149 cultured cortical neurons at 15 day *in-vitro* (DIV 15) using luciferase-based methods.

150 (**B**) Bar graph representing normalized average value of neuronal ATP/ATP+ADP ratio in
151 unstimulated condition, in presence of Anisomycin (25μM), cycloheximide (350μM), on
152 glutamate (25μM) stimulation alone for 5 minutes, on glutamate stimulation along with
153 anisomycin, on glutamate stimulation along with cycloheximide and on glutamate stimulation
154 in combination with D-AP5, CNQX and anisomycin. Data represented as: mean ± SEM with
155 scattered data points. *$p<0.05$, n=3-6 independent plating. One-way ANOVA followed by
156 Bonferroni's multiple comparison test.

157 (**C**) Bar graph representing normalized average value of neuronal ATP/ATP+ADP ratio in
158 unstimulated condition, in presence of MPEP (10μM), in presence of the cocktail of CNQX (40μM)
159 + D-AP5 (25μM), on glutamate (25μM) stimulation alone for 5 minutes, on glutamate stimulation
160 along with the cocktail of CNQX + D-AP5 and on glutamate stimulation along with MPEP. Data
161 represented as: mean ± SEM with scattered data points. *$p<0.05$, **$p<0.01$, ***$p<0.001$, n=3-5
162 independent plating. One-way ANOVA followed by Bonferroni's multiple comparison test.

163 **(D)** Schematic depicting experimental work flow for measurement of synaptic ATP level from
164 cortical synaptoneurosomes obtained from Sprague dawley rats at post-natal day 30 (P30) using
165 luciferase-based methods.

166 **(E)** Immunoblots showing PSD 95 and GFAP levels on whole cortical lysate and
167 synaptoneurosome preparation. Quantification representing average fold enrichment of PSD 95
168 and GFAP on synaptoneurosome preparations compared to whole cortex lysate.

169 **(F)** Bar graph representing normalized average value of synaptic ATP level in unstimulated
170 condition, on DHPG (100μM) treatment for 5 minutes, on DHPG treatment along with MPEP
171 (10μM), on DHPG treatment along with anisomycin (50μM), on DHPG treatment along with
172 cycloheximide (350μM), on NMDA (40μM) treatment for 5 minutes and on NMDA treatment along
173 with D-AP5 (25μM). Data: mean +/- SEM with scattered data points. *$p<0.05$, n=5-10
174 independent plating. One-way ANOVA followed by Bonferroni's multiple comparison test.

175 **mGluRs and NMDARs impact synapto-dendritic ATP levels with distinct kinetics**

176 To understand the kinetics of activity induced changes in energy level at a more
177 compartment specific manner, we measured ATP/ADP ratio following mGluR and
178 NMDAR stimulation at the distal dendrites of cortical neurons (~50μm away from cell
179 body) using ratio sensor PercevalHR as reported previously [23] (**Figure 2A**). Perceval pH
180 bias was approximately corrected by simultaneous measurement of intracellular pH
181 with the ratio sensor pH-Red using the linear relation between Perceval and pH-Red
182 fluorescence as described previously [2423] **(supplementary figure 2A)**. On bath
183 application of 50μM DHPG (mGluR agonist) we observed a rapid and significant
184 reduction (~ by 2 mins) in the dendritic ATP/ADP ratio. The ratio continued to stay low
185 long as DHPG was present in the media (**Figure 2B-2E**). Application of NMDA (20μM) on
186 bath conversely showed much delayed (~10 minutes post-stimualtion) reduction in the
187 ratio indicating a slow kinetics of NMDAR effect on dendritic ATP:ADP ratio distinctly
188 different to that of mGluRs (**Figure 2B-2E)**. Stimulation in presence of protein synthesis

189 inhibitor anisomycin inhibited the activity dependent reduction in the dendritic
190 ATP/ADP ratio for both DHPG and NMDA treatment (**Figure 2C-2F**). While the dendritic
191 ATP/ADP ratio was unaltered under basal condition, application of anisomycin led to a
192 sharp rise in ATP/ADP ratio reflecting the energy consumption due to basal protein
193 synthesis (**supplementary figure 2B and 2C**). Our observations therefore clearly
194 indicate that stimulation dependent protein synthesis is a major energy burden even at
195 the local dendritic compartments.

196 To investigate the kinetics of ATP regulation at the synapse we used cortical
197 synaptoneurosome preperation. We stimulated synaptoneurosomes for 1, 2 and, 5
198 minutes and allowed recovery for 5 minutes after stimulation (hence reffered to as 5
199 min recovery hereafter). ATP levels were quantified from the specified time points
200 using luminescence-based methods from synaptoneurosomal lysates (**Figure 2F**). DHPG
201 (100μM) addition alone led to a rapid and significant reduction of the synaptic ATP level
202 at 2 minutes and 5 minutes after stimulation and reached baseline at 5 min recovery
203 time point. The DHPG induced changes in synaptic ATP levels was lost in presence of
204 anisomycin highlighting most of the change in the ATP level was contributed by protein
205 synthesis (**Figure 2G**). NMDA stimulation in the same system had no significant impact
206 on the ATP levels till 5 minutes of stimulation but exhibited a significant reduction at
207 5 min recovery time point. Stimulation in presence of anisomycin had no additional
208 effect as that of NMDAR alone (**Figure 2H**) suggesting no detectable amount of protein
209 synthesis happened till 5 minutes of NMDAR stimulation [16]. Synaptic ATP level was
210 unaltered in absence of any stimulation for a period similar as stimulations
211 (**supplementary figure 2D**). Together our results indicate mGluR stimulation leads to a

212 rapid and persistent reduction in ATP level in a protein synthesis dependent manner

213 while NMDAR stimulation impacts ATP level with a late onset of protein synthesis.

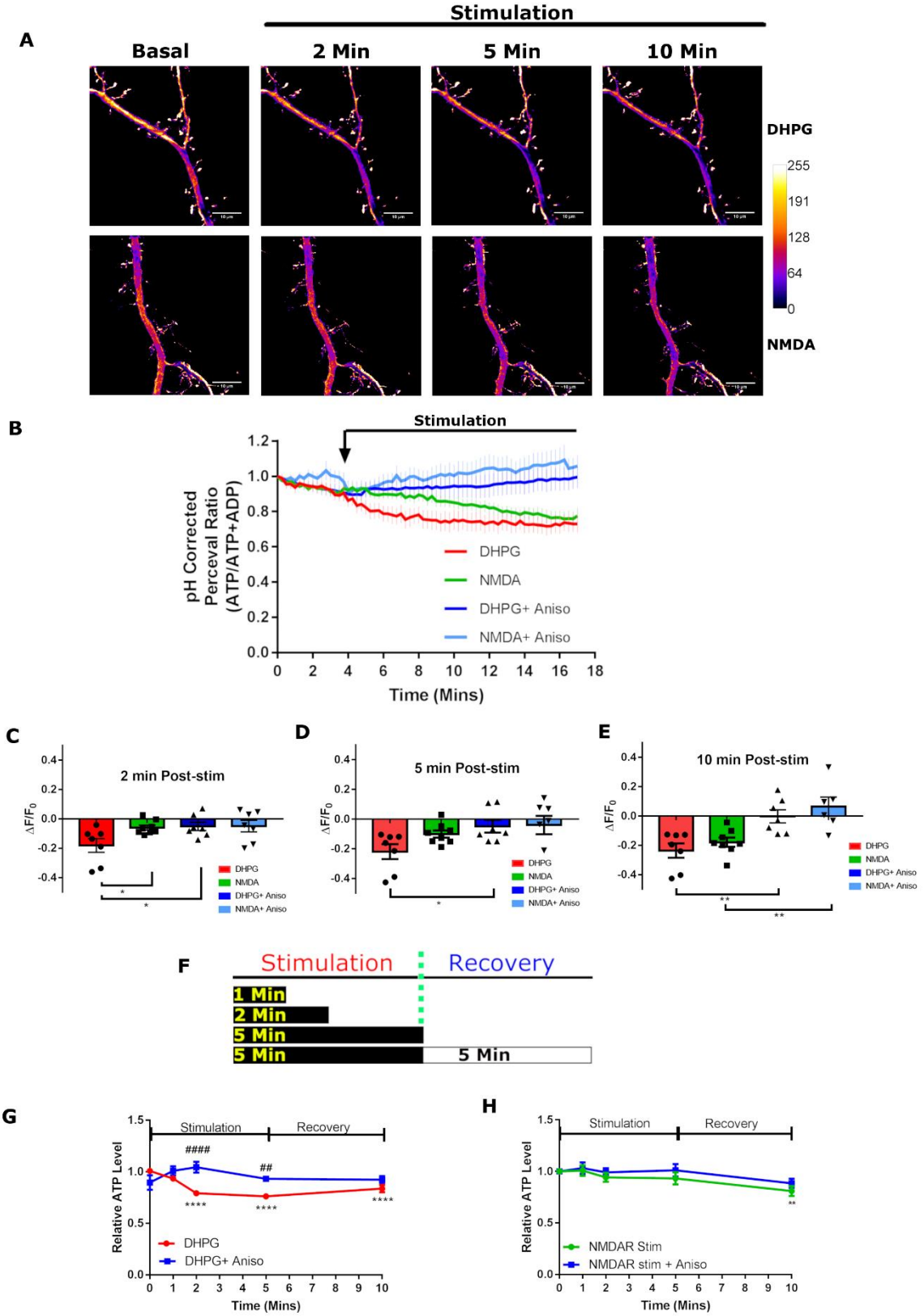
A
Stimulation
Basal
2 Min
5 Min
10 Min
DHPG
255
191
128
64
0
NMDA
B
Stimulation
pH Corrected Perceval Ratio (ATP/ATP+ADP)
DHPG
NMDA
DHPG+ Aniso
NMDA+ Aniso
Time (Mins)
C
2 min Post-stim
D
5 min Post-stim
E
10 min Post-stim
ΔF/F0
F
Stimulation
Recovery
1 Min
2 Min
5 Min
5 Min
5 Min
G
Stimulation
Recovery
Relative ATP Level
DHPG
DHPG+ Aniso
Time (Mins)
H
NMDAR Stim
NMDAR stim + Aniso

214

215 **Legend for Figure 2**

216 **mGluR and NMDAR impacts dendritic ATP/ADP ratio with distinct Kinetics.**

217 **(A)** Representative dendrite showing changes on PercevalHR fluorescence ratio (~ATP/ADP
218 ratio) on bath application of DHPG (50μM) and NMDA (20μM). Scale=10μM.

219 **(B)** Average time traces showing the changes in the dendritic ATP/ADP ratio on DHPG and NMDA
220 treatment in presence or absence of anisomycin (25μM). The curved arrow on top indicates the
221 time when stimulants were added and kept in the imaging media. Data: mean +/- SEM, n= 6-8
222 cells from independent plating.

223 **(C)** Bar graph representing average change in PercevalHR fluorescence (ΔF/F) on DHPG
224 treatment, NMDA treatment, DHPG treatment along with anisomycin and NMDA treatment along
225 with anisomycin 2 minutes after stimulant was added on bath. Data: mean +/- SEM. *$p<0.05$,
226 n= 6-8 cells from independent plating. One Way ANOVA followed by Bonferroni's multiple
227 comparison test.

228 **(D)** Bar graph representing average change in PercevalHR fluorescence (ΔF/F) on DHPG
229 treatment, NMDA treatment, DHPG treatment along with anisomycin and NMDA treatment along
230 with anisomycin 5 minutes after stimulant was added on bath. Data: mean +/- SEM. *$p<0.05$,
231 n= 6-8 cells from independent plating. One Way ANOVA followed by Bonferroni's multiple
232 comparison test.

233 **(E)** Bar graph representing average change in PercevalHR fluorescence (ΔF/F) on DHPG
234 treatment, NMDA treatment, DHPG treatment along with anisomycin and NMDA treatment along
235 with anisomycin 2 minutes after stimulant was added on bath. Data: mean +/- SEM. **$p<0.01$,
236 n= 6-8 cells from independent plating. One Way ANOVA followed by Bonferroni's multiple
237 comparison test.

238 **(F)** Schematic depicting stimulation protocol in cortical synaptoneurosomes for quantification
239 synaptic ATP levels.

240 **(G)** Line graph showing average synaptic ATP levels at various time points after DHPG (100μM)
241 treatment and 5 minutes after recovery in presence or absence of anisomycin (50μM). Data:
242 mean +/- SEM, *p<0.05, **p<0.01, ****p<0.0001 for comparison with 0 minute. ##p<0.01 and
243 ####p<0.0001 for comparison between DHPG+aniso. n≥ 5 animals per group. Two Way ANOVA
244 followed by Bonferroni's multiple comparison test.

245 **(H)** Line graph showing average synaptic ATP levels at various time points after NMDA (40μM)
246 treatment and 5 minutes after recovery in presence or absence of anisomycin (50μM). Data:
247 mean +/- SEM, **p<0.01 for comparison with 0 minute. n≥ 4 animals per group. Two Way ANOVA
248 followed by Bonferroni's multiple comparison test

249

250 **mGluRs and NMDARs regulate eEF2 phosphorylation to create distinct kinetics of**
251 **translation**

252 To understand the stimulation dependent changes on global translation with a direct
253 correlate, we quantified de-novo protein synthesis at various time points after
254 stimulation using FUNCAT metabolic labeling technique as described previously [25].
255 Cultured cortical neurons (DIV 15) were methionine starved for 1 hour followed by
256 application of methionine analogue AHA and incubation for 1 hour for abundant labeling
257 of proteins. This was followed by stimulation as described in figure 2F and fixation
258 (**Figure 3A**). Newly synthesized proteins were visualized by tagging the AHA containing
259 proteins with Alexa 555 alkyn. Mean FUNCAT intensity was then quantified from somata
260 and dendrites representing quantity of proteins synthesized cumulatively over the

261 period of stimulation (**Figure 3B, 3C, 3D and supplemenatry figure 3B**). On bath
262 application of DHPG, we did not observed any discernable change in the FUNCAT signal
263 by 2 minutes. The signal increased significantly though by 5 minutes and by 5 min
264 recovery as compared to unstimulated cells. This demonstrates a robust and persistent
265 increase in de-novo protein synthesis on mGluR stimulation in cultured cortical neurons
266 (**Figure 3C and 3D**). On the contrary NMDA stimulation led to a significant reduction in
267 FUNCAT signal compared to unstimulated cells by 2 minutes while the signal intensity
268 returned to baseline by 5 minutes of stimulation and continued to stay unchanged till
269 5 min recovery (**Figure 3C and 3D**) indicating a a rapid inhibition of translation on
270 NMDAR stimulation following. No significant change in FUNCAT signal was observed in
271 absence of any stimulation (**supplementary figure 3A**). No detectable signal was
272 observed in absence of any AHA incubation which acted as a negative control for our
273 experiment (**supplementary figure 3A**). Therefore, our observations reveal a robust
274 and persistent activation of translation mediated by mGluRs while NMDAR stimulation
275 led to a rapid inhibition of translation.

276 Eukaryotic elongation factor 2 (eEF2) has been proposed to be a signal integrator [26] and
277 its phosphorylation is known to respond to various synaptic stimuli [1627] thereby
278 regulating translation elongation [28]. Phosphorylation of Thr 56 residue of eEF2 is known
279 to pause translation elongation thereby causing global translation inhibition [29]. To gain
280 insight on the modes of translation regulation downstream of both receptors, we
281 decided to investigate on the role of elongation factor 2 (eEF2) phosphorylation in
282 cultured cortical neurons. We quantified eEF2 phosphorylation 5 minutes after
283 stimulation, a time point corresponding to maximum difference observed in FUNCAT

284 signal (**Figure 3E and Supplementary figure 3C**). We observed a significant reduction
285 in p-eEF2 levels 5 minutes after DHPG treatment as compared to unstimulated cells.
286 NMDA treatment on the contrary robustly increased the p-eEF2 levels in the cell somata
287 and dendrites (**Figure 3F**). Further we used phospho/ total ratio of eEF2 as a readout
288 to gain a snapshot view of global translation in cortical synaptoneurosomes (**Figure 3G**)
289 and in cortical neurons (**supplementary figure 3D**). Synaptoneurosomes were
290 stimulated for different time period as mentioned before (**Figure 2F**). We observed a
291 significant difference in the kinetics of eEF2 phosphorylation regulated by mGluR and
292 NMDAR stimulation (**Figure 3H and supplementary figure 3E**). mGluR stimulation led
293 to an immediate reduction in phospho/total eEF2 ratio by 1 minute. The decrease in
294 the ratio persisted till 5 minutes of stimulation and returned to baseline by 5 mins of
295 recovery. NMDAR stimulation, on the contrary lead to an immediate increase in the
296 phospho/Total eEF2 ratio by 1 minute correlated well with the decrease in FUNCAT
297 signal observed 2 minutes after stimulation in cortical neurons. The increase in the ratio
298 persisted till 5 minutes of NMDAR stimulation and returned to baseline by 5 min recovery
299 time point (**Figure 3H**). The ratio stayed unaltered in absence of any stimulation
300 (**supplementary figure 4B**). Therefore, we found a strong correlation between the
301 global translation and eEF2 phosphorylation downstream of both the glutamate
302 receptor stimulation.

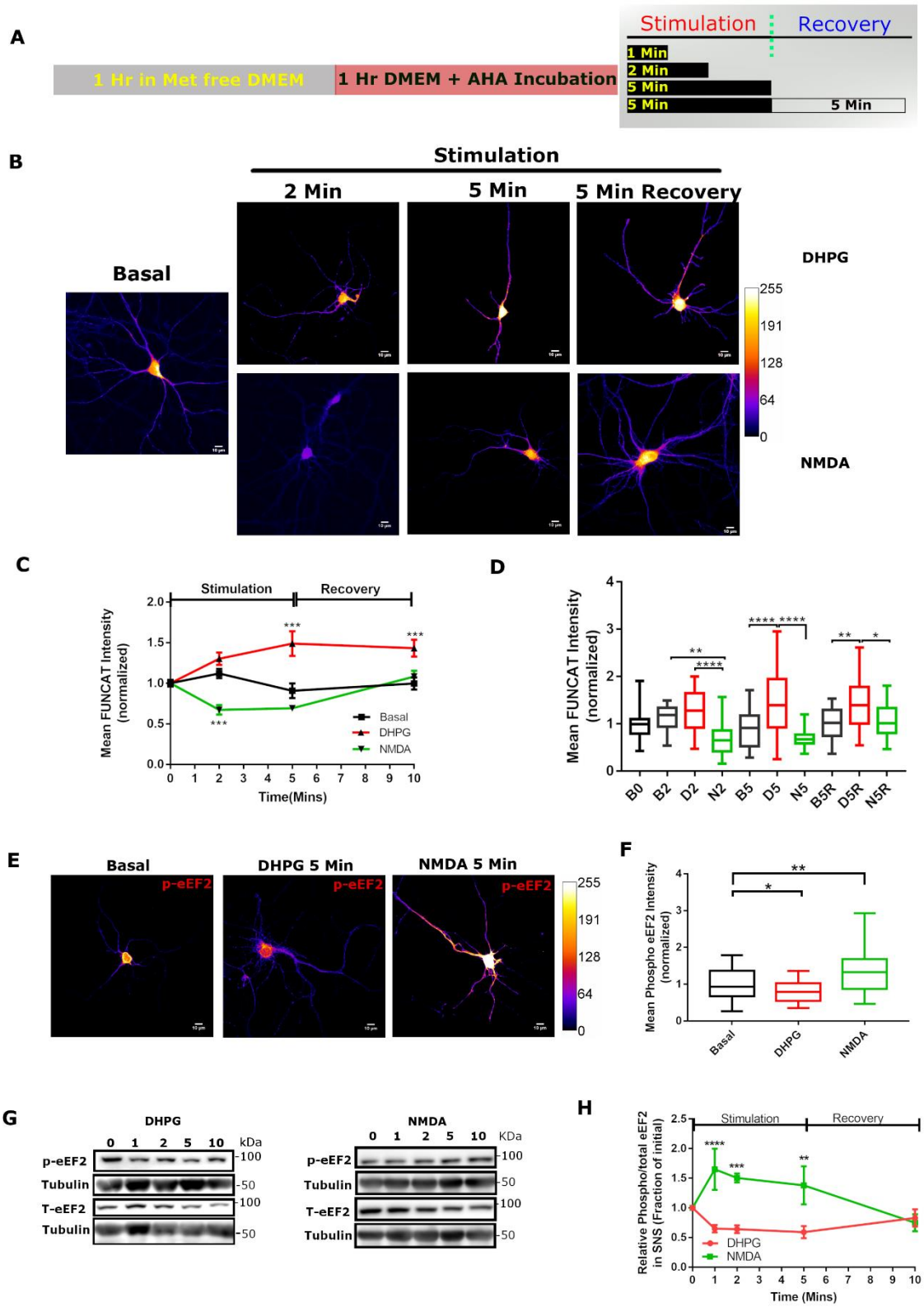
A
1 Hr in Met free DMEM
1 Hr DMEM + AHA Incubation
Stimulation
Recovery
1 Min
2 Min
5 Min
5 Min
5 Min
B
Stimulation
2 Min
5 Min
5 Min Recovery
Basal
DHPG
NMDA
255
191
128
64
0
C
Stimulation
Recovery
Mean FUNCAT Intensity (normalized)
Time(Mins)
Basal
DHPG
NMDA
D
Mean FUNCAT Intensity (normalized)
B0
B2
D2
N2
B5
D5
N5
B5R
D5R
N5R
E
Basal
DHPG 5 Min
NMDA 5 Min
p-eEF2
255
191
128
64
0
F
Mean Phospho eEF2 Intensity (normalized)
Basal
DHPG
NMDA
G
DHPG
0 1 2 5 10 kDa
p-eEF2
Tubulin
T-eEF2
Tubulin
100
50
100
50
NMDA
0 1 2 5 10 KDa
p-eEF2
Tubulin
T-eEF2
Tubulin
100
50
100
50
H
Stimulation
Recovery
Relative Phospho/total eEF2 in SNS (Fraction of initial)
DHPG
NMDA
Time (Mins)

304 **Legend for Figure 3:**

305 **mGluR and NMDAR alter global translation by regulating eEF2 phosphorylation with distinct**
306 **kinetics.**

307 **(A)** Schematic depicting the experimental workflow and stimulation protocol to visualize and
308 quantify newly synthesized protein on stimulation through metabolic labeling technique in
309 cortical neurons DIV 15.

310 **(B)** Representative images showing newly synthesized proteins visualized through FUNCAT
311 metabolic labeling (pseudo-colored) in cortical neurons at various time points following DHPG
312 (50μM) and NMDA (20μM) treatment. MAP2B immunolabeling (supplementary figure 3B) was
313 used for identifying neurons and intensity was used for normalization. Scale=10μM.

314 **(C)** Line graph showing average newly synthesized protein intensity before stimulation (basal)
315 and at various time points following DHPG and NMDA treatments. Data: mean +/- SEM,
316 ***$p<0.001$ n= 21-54 neurons per group from 3 independent plating. Two Way ANOVA followed
317 by Bonferroni's multiple comparison test.

318 **(D)** Box plot showing distribution of data points for the newly synthesized protein obtained from
319 various neurons for each group. *$p<0.05$, **$p<0.01$, ***$p<0.001$, ****$p<0.0001$, n= 21-54 neurons
320 per group from 3 independent plating. One Way ANOVA followed by Bonferroni's multiple
321 comparison test.

322 **(E)** Representative images showing phospho-eEF2 immunolabeling (Pseudo-colored) in cortical
323 neurons on basal, DHPG and NMDA treatments for 5 minutes. MAP2B immunolabeling
324 (supplementary figure 3C) was used for identifying neurons and intensity was used for
325 normalization. Scale=10μM.

326 **(F)** Box plot showing phospho-eEF2 intensity distribution across multiple neurons on basal
327 condition and on DHPG and NMDA treatment for 5 minutes. *p<0.05, **p<0.01, n=31-49 cells per
328 group from 3 independent plating. One-way ANOVA followed by Bonferroni's multiple
329 comparison test.

330 **(G)** Representative immunoblots describing changes in phospho-eEF2 and total-eEF2 levels at
331 various time points after DHPG (100μM) and NMDA (40μM) treatment to cortical
332 synaptoneurosomes. Note in each case phospho and total eEF2 levels were normalized
333 individually to tubulin before calculating the ratio.

334 **(H)** Line graph showing average value for synaptic phospho/total ratio of eEF2 at various time
335 points after DHPG and NMDA treatment and 5 minutes after recovery. Data: mean +/- SEM,
336 **p<0.01, ***p<0.001, ****p<0.0001, n≥ 5 animals per group. Two Way ANOVA followed by
337 Bonferroni's multiple comparison test.

338 **mGluRs and NMDARs regulate AMPK activity in contrasting manner**

339 AMP activated protein kinase (AMPK) is a widely studied global sensor for ATP/AMP or
340 ADP ratio and is known to regulate various catabolic and anabolic processes during
341 energy stress [20]. Since mGluRs and NMDARs had contrasting effect on both ATP/ADP
342 ratio and global translation, we sought to understand if AMPK activity was altered to
343 achieve stimulation specific effects. To examine the global status of AMPK activity we
344 quantitated T172 phosphorylation on AMPK α subunit 5 minutes after stimulation in
345 cortical neurons through immunolabeling (DIV 15) (**Figure 4A and supplementary**
346 **figure 4A**). T172 is present in the activation loop of AMPK and its phosphorylation is
347 positively correlated with heightened AMPK activation [30] (Hawley et al., 1996,). We
348 observed a significant decrease in p-AMPK immunolabeling on mGluR stimulation

349 compared unstimulated condition. NMDAR stimulation on the contrary led to a
350 significant rise in the immunolabel indicating an increase in AMPK activity (**Figure 4B**).
351 To understand the temporal changes in AMPK activity, we stimulated cortical
352 synaptoneurosomes with DHPG followed by measurement of phospho/total AMPK ratio
353 (**Figure 4C**). We found a significant decrease in the ratio by about 2 minutes after DHPG
354 treatment persisting till 5 minutes of recovery (**Figure 4D**) while the ratio stayed
355 unaltered in absence of any stimulation (**supplementary figure 4B**). These results
356 indicate that AMPK activity underwent reduction on mGluR stimulation despite an
357 observed decline in the ATP level. Surprisingly, the mGluR mediated reduction in AMPK
358 activity was found to be abolished in presence of anisomycin underscoring the
359 importance of de-novo protein synthesis in regulation of AMPK activity (**Figure 4C and**
360 **4D)**. One pressing idea was therefore to test whether mGluR stimulation leads to
361 synthesis of any protein that would inhibit AMPK phosphorylation. We chose α-SNAP as
362 a potential candidate to investigate, a *cis*-SNARE disassembly factor, reported to act as
363 a phosphatase of AMPK [31]. We investigated the α-SNAP protein level on DHPG treatment
364 in cortical synaptoneurosomes (**Figure 4E**). A significant increase in α-SNAP level was
365 observed on 1 min of DHPG addition and was persistent till 5 min recovery (**Figure 4F**),
366 a temporal feature well correlated with AMPK inactivation kinetics (**Figure 4D**). The
367 DHPG induced increase in α-SNAP level was found to be abolished in presence of protein
368 synthesis inhibitor anisomycin indicating mGluR dependent de-novo synthesis of α-SNAP
369 plays critical role in AMPK dephosphorylation (**Figure 4F**). Further We quantified the
370 association between α-SNAP and AMPK on mGluR stimulation in cortical cultured
371 neurons (**Figure 4G**) as α-SNAP is known to stabilize the de-phosphorylated version of

372 AMPK. We observed a significant increase in colocalization between α-SNAP and AMPK
373 in cortical neurons after DHPG treatment (5 minutes) compared to unstimulated
374 condition (**Figure 4H**). These results therefore suggest a crucial role for protein α-
375 SNAP in mediating mGluR mediated dephosphorylation of AMPK.

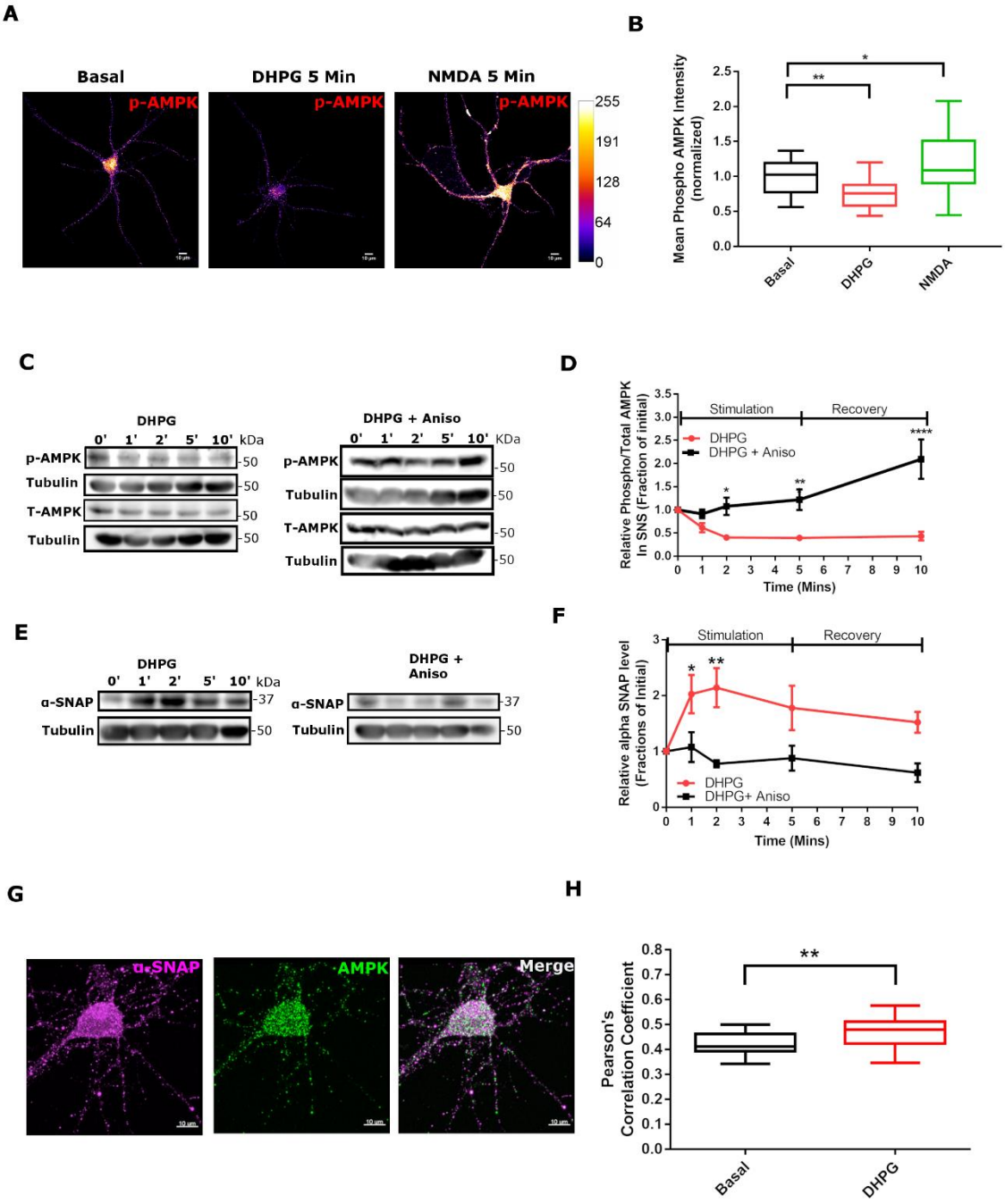
A
Basal
DHPG 5 Min
NMDA 5 Min
p-AMPK
255
191
128
64
0
B
Mean Phospho AMPK Intensity (normalized)
Basal
DHPG
NMDA
C
DHPG
DHPG + Aniso
0' 1' 2' 5' 10' kDa
p-AMPK
Tubulin
T-AMPK
D
Relative Phospho/Total AMPK In SNS (Fraction of initial)
Stimulation
Recovery
DHPG
DHPG + Aniso
Time (Mins)
E
α-SNAP
F
Relative alpha SNAP level (Fractions of Initial)
DHPG+ Aniso
G
α-SNAP
AMPK
Merge
H
Pearson's Correlation Coefficient

377 **Legend for Figure 4:**

378 **mGluR inhibit while NMDAR activate AMPK to regulate translation.**

379 **(A)** Representative images showing phospho-AMPK immunolabeling (Pseudo-colored) in cortical
380 neurons on basal, DHPG and NMDA treatments for 5 minutes. MAP2B immunolabeling
381 (supplementary figure 4A) was used for identifying neurons and intensity was used for
382 normalization. Scale=10μM.

383 **(B)** Box plot showing phospho-AMPK intensity distribution across multiple neurons on basal
384 condition and on DHPG and NMDA treatment for 5 minutes. *$p<0.05$, **$p<0.01$, n=30-46 cells per
385 group from 3 independent plating. One-way ANOVA followed by Bonferroni's multiple
386 comparison test.

387 **(C)** Representative immunoblots describing changes in phospho-AMPK and total-AMPK levels at
388 various time points after DHPG (100μM) treatment to cortical synaptoneurosomes in presence
389 or absence of anisomycin (50μM). Note in each case phospho and total AMPK levels were
390 normalized individually to tubulin before calculating the ratio.

391 **(D)** Line graph showing average value for synaptic phospho/total ratio of AMPK at various time
392 points after DHPG treatment and 5 minutes after recovery in presence or absence of
393 anisomycin. Data: mean +/- SEM, *$p<0.05$, **$p<0.01$, ****$p<0.0001$, n= 5 animals per group. Two
394 Way ANOVA followed by Bonferroni's multiple comparison test.

395 **(E)** Representative immunoblots depicting changes in α-SNAP levels at various time points after
396 DHPG treatment to cortical synaptoneurosomes in presence or absence of anisomycin.

397 **(F)** Line graph showing average value for synaptic α-SNAP levels at various time points after
398 DHPG treatment and 5 minutes after recovery in presence or absence of anisomycin. Data:

399 mean +/- SEM. *p<0.05, **p<0.01, n≥ 4 animals per group. Two Way ANOVA followed by
400 Bonferroni's multiple comparison test.

401 **(G)** Representative images showing α-SNAP (green) and AMPK (red) immunolabeling in cortical
402 neurons. Merge shows the colocalization of two channels. Scale=10μM.

403 **(H)** Box plot depicting quantification of co-localization between -SNAP and AMPK in cortical
404 neurons under basal and DHPG treated conditions. **p<0.01, n≥24 cells per group from 3
405 independent plating. Unpaired-sample t test.

406 **NMDAR Regulate AMPK Activity in Ca2+ dependent Manner**

407 We further investigated the kinetics and mechanism of NMDAR mediated AMPK
408 regulation in cortical synaptoneurosomes (**Figure 5A**). We observed a rapid increase in
409 phospho/total AMPK ratio by 1 minute of stimulation and persisting till 5 mins recovery
410 (**Figure 5B**). This observation is in parallel to our previous observation in neurons where
411 NMDA stimulation lead to enhanced phosphorylation of AMPK (**Figure 4B**). Interestingly
412 we did not observe any detectable change in ATP level (**Figure 2I**) at a similar time
413 scale hinting towards an ATP independent regulation of AMPK. CamKIIß, one of the
414 upstream kinases of AMPK [20](Burkewitz et al. 2014), is known to phosphorylate it in a
415 Ca^{2+} dependent and ATP independent manner. Therefore, we hypothesized that NMDAR
416 dependent increase in AMPK function is mediated by increased cytosolic Ca^{2+} levels
417 entered through open NMDARs. To test the hypothesis, we repeated NMDAR stimulation
418 in absence of extracellular Ca^{2+} (**Figure 5A**). We observed a significantly different AMPK
419 response on NMDA treatment in absence of extracellular Ca^{2+} (**Figure 5B**). The
420 stimulation dependent increase in phospho/total AMPK ratio was absent in Ca^{2+} free
421 buffer underscoring the importance of Ca^{2+} signaling in this context. Interestingly we

422 observed the NMDA dependent increase in phspho/total eEF2 level was also abolished
423 in absence of extracellular Ca^{2+} (**supplemenatary figure 4D**) clearly demonstrating the
424 importance of Ca^{2+} dependent signaling mechanism in NMDAR dependent translation
425 regulation.

426 We further followed the kinetics of NMDAR mediated Ca^{2+} entry in cortical neurons.
427 Cytosolic free Ca^{2+} level was quantified on NMDAR stimulation using fluorescent based
428 Ca^{2+} probe Fluo-8AM. We observed a rapid increase in Fluo8 fluorescence on NMDA
429 addition and persisted till the presence of stimulant in the media (**Figure 5C, 5F and**
430 **5G**) indicating an increase in intracellular Ca^{2+} on NMDA treatment. The amount of Ca2+
431 entered was non-saturating as could be inferred from further increase in fluorescence
432 on addition of ionomycin in presence of 10mM Ca^{2+} (**Figure 5F**). The observed increase
433 in Ca^{2+} is NMDA specific as pre-treatment with D-AP5 abolished the rise in Ca^{2+} (**Figure**
434 **5D, 5F and 5G**). The Ca^{2+} surge is contributed primarily by synaptic NMDARs as the
435 response was observed to be absent in presence of MK801 (10μM), a compound known
436 to block the open NMDAR channel pores (**supplementary figure 4C; Figure 5G**). The
437 rise in fluorescence on stimulation was abolished in the absence of extracellular Ca^{2+}
438 indicating the source of the ions are majorly extracellular in nature (**Figure 5E, 5F and**
439 **5G**). Therefore, our results indicate NMDAR mediated rapid entry of external Ca^{2+} is
440 responsible for rapid AMPK activation.

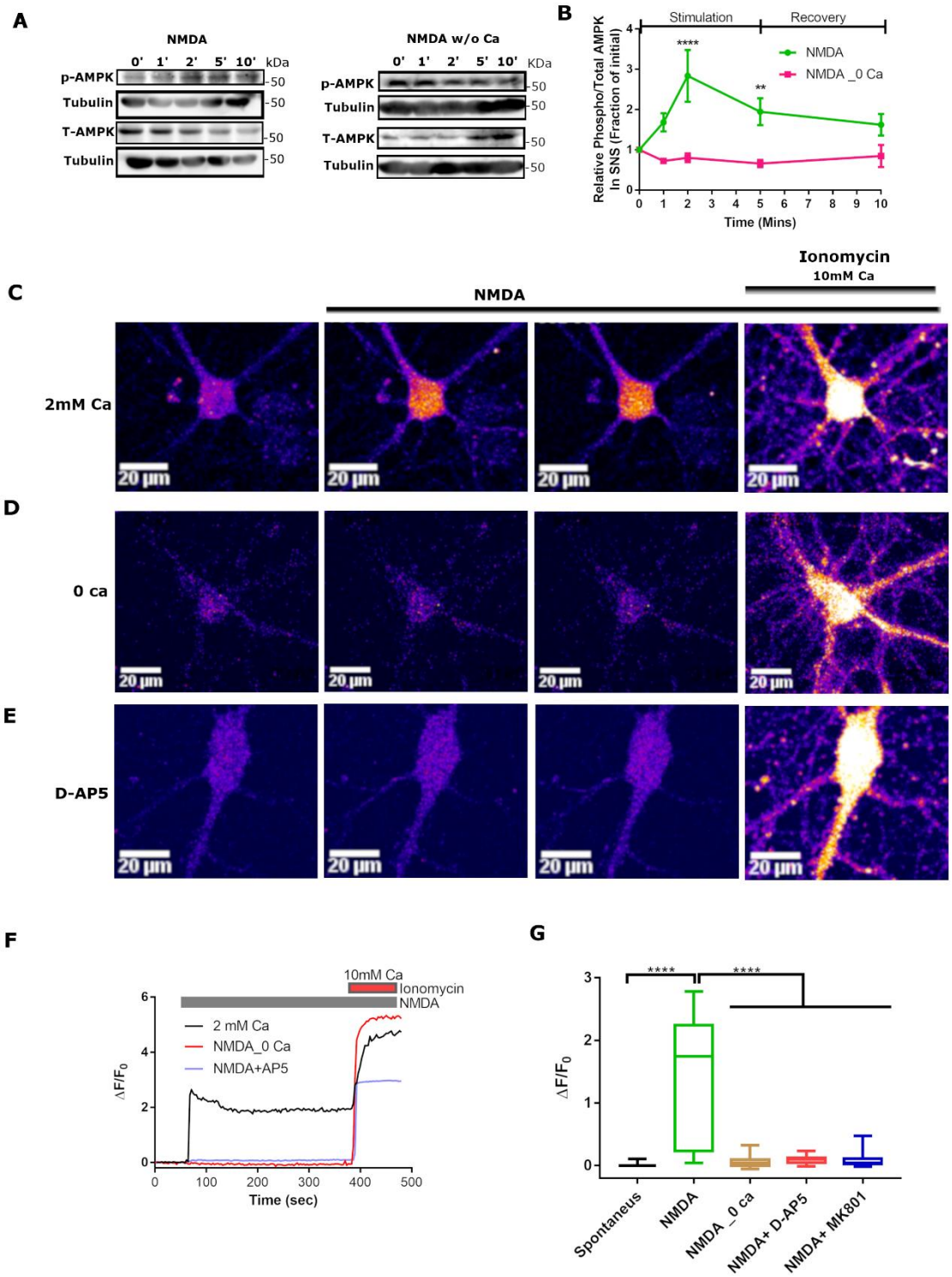
A
NMDA
0' 1' 2' 5' 10' kDa
p-AMPK
Tubulin
T-AMPK
Tubulin
50
NMDA w/o Ca
B
Stimulation
Recovery
NMDA
NMDA _0 Ca
Relative Phospho/Total AMPK In SNS (Fraction of initial)
Time (Mins)
Ionomycin
10mM Ca
C
NMDA
2mM Ca
D
0 ca
E
D-AP5
20 µm
F
10mM Ca
Ionomycin
NMDA
2 mM Ca
NMDA_0 Ca
NMDA+AP5
ΔF/F0
Time (sec)
G
Spontaneus
NMDA
NMDA _0 ca
NMDA+ D-AP5
NMDA+ MK801

441

442 **Legend for Figure 5:**

443 **NMDAR mediated AMPK activation is extracellular calcium dependent.**

444 **(A)** Representative immunoblots describing changes in phospho-AMPK and total-AMPK levels at
445 various time points after NMDA (40μM) treatment to cortical synaptoneurosomes in presence or
446 absence of extracellular Ca^{2+}. Note in each case phospho and total AMPK levels were normalized
447 individually to tubulin before calculating the ratio.

448 **(B)** Line graph showing average value for synaptic phospho/total ratio of AMPK at various time
449 points after NMDA treatment and 5 minutes after recovery in presence or absence of
450 extracellular Ca^{2+}. Data: mean +/- SEM, **$p<0.01$, ****$p<0.0001$, n= 6 animals per group. Two
451 Way ANOVA followed by Bonferroni's multiple comparison test.

452 **(C,D,E)** Representative images depicting intracellular Ca^{2+} levels (Pseudo-colored) of a cortical
453 neuron before stimulation, immediately (15s) after NMDA (20μM) treatment, at a later time
454 point (300sec) after NMDA treatment and after ionomycin treatment along with 10mM Ca^{2+} in
455 presence or absence of extracellular Ca^{2+} and D-AP5. Scale=20μM.

456 **(F)** Representative time trace showing the change in Fluo8 fluorescence on NMDA treatment in
457 presence or absence of extracellular Ca^{2+} and D-AP5. Ionomycin treatment in presence of 10mM
458 Ca^{2+} was used to calculate fluorescence maximum for a particular cell.

459 **(F)** Box plot showing the distribution of $\Delta F/F_0$ across multiple neurons under spontaneously
460 firing condition, on NMDA treatment in presence or absence of Ca^{2+}, on NMDA treatment along
461 with D-AP5 (25μM) and on NMDA treatment along with MK-801. ****$p<0.0001$, $n\geq30$ neurons per
462 group from 3 independent plating. One-way ANOVA followed by Bonferroni's multiple
463 comparison test.

464 **Perturbation of AMPK function disrupts mGluR and NMDAR specific translation**
465 **response**

466 We present two key pieces of experimental evidence to verify the idea that tight
467 regulation of AMPK function is necessary to generate receptor specific translation
468 response. Since mGluR activation lead to inhibition of AMPK function, first we
469 hypothesized that acute activation of AMPK with 5-aminoimidazole-4-carboxamide
470 ribonucleotide (AICAR; 1mM) should preclude the mGluR specific effect on translation.
471 AICAR treatment alone led to significant increase in p-eEF2 levels (**Figure 6B,**
472 **supplementary 5A)** without any significant alteration in FUNCAT signal (**Figure 6D,**
473 **supplementary 5A**) in cortical neurons. These observations establish a direct influence
474 imparted by AMPK on eEF2 phosphorylation and on global translation. Supporting this
475 hypothesis, DHPG mediated reduction in p-eEF2 level was abolished in presence of
476 AICAR (**Figure 6A,B, supplementary figure 5B**) and DHPG induced increase in global
477 translation was absent in presence of AICAR (**Figure 6C,D, supplementary figure 5B**).
478 Next, we examined the impact of AMPK inhition on NMDAR stimulation using AMPK
479 inhibitor Compund C (Dorsomorphin). Blocking AMPK function with Compound C
480 (Dorsomorphin) had no significant impact on basal p-eEF2 level (**6F, supplementary**
481 **5A**) and but led to a significant increase FUNCAT signal (**6H, supplementary 5A**).
482 Interestingly, NMDA application in presence of Compound C completely abolished the
483 NMDA mediated increase in p-eEF2 level (**Figure 6E,F, supplementary figure 5C**) and
484 also diminished the NMDA mediated inhibition of global translation (**Figure 6G,H,**
485 **supplementary figure 5C**). These observations therefore, establish the strong influence

486 of AMPK over receptor mediated translation regulation and highlights the importance

487 of AMPK-eEF2 signaling axis in the same context.

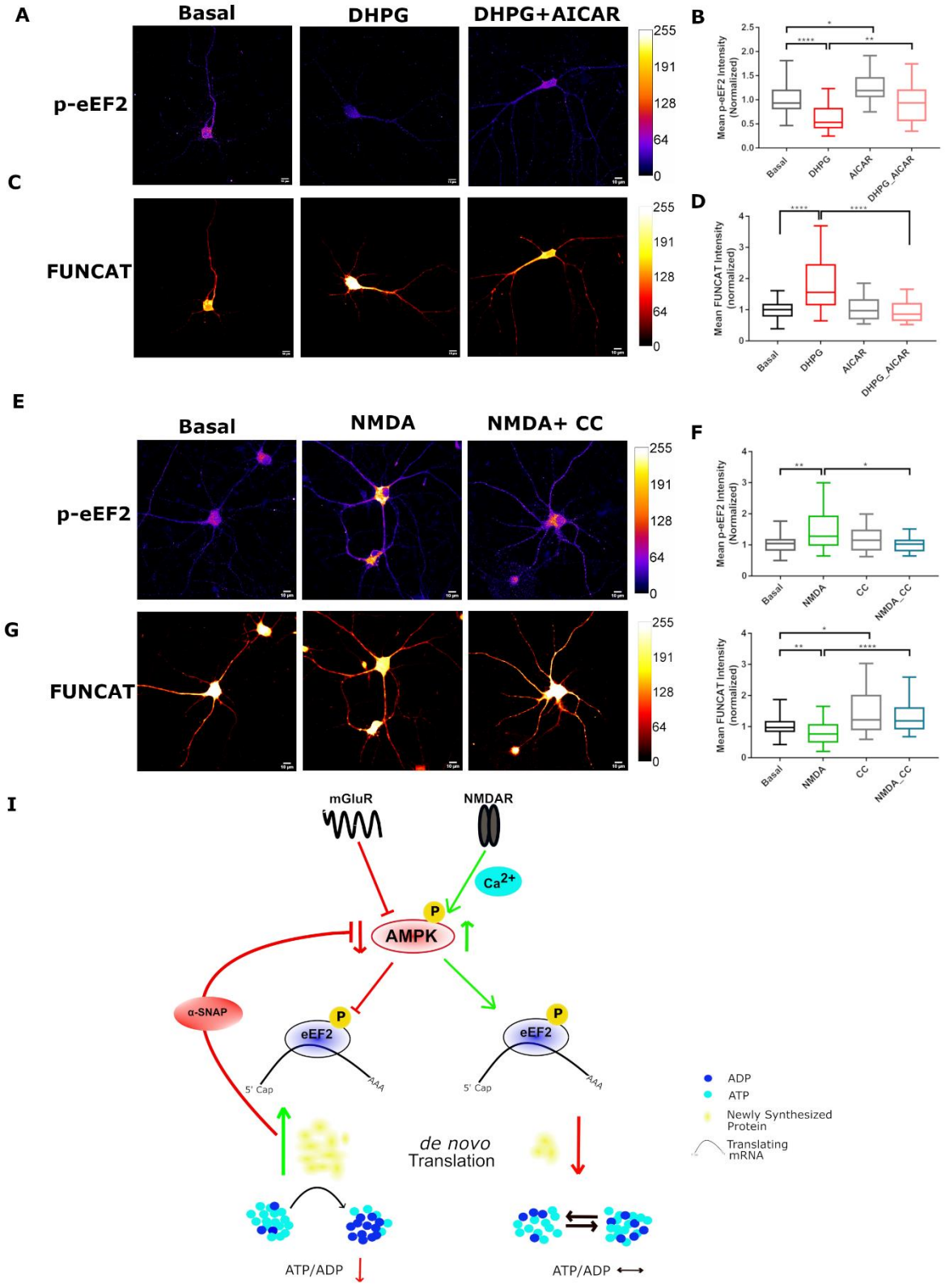
A
Basal
DHPG
DHPG+AICAR
p-eEF2
255
191
128
64
0
B
Mean p-eEF2 Intensity (Normalized)
Basal
DHPG
AICAR
DHPG_AICAR
C
FUNCAT
D
Mean FUNCAT Intensity (normalized)
E
Basal
NMDA
NMDA+ CC
p-eEF2
F
Mean p-eEF2 Intensity (Normalized)
Basal
NMDA
CC
NMDA_CC
G
FUNCAT
Mean FUNCAT Intensity (normalized)
I
mGluR
NMDAR
Ca2+
P
AMPK
α-SNAP
eEF2
5' Cap
AAA
de novo Translation
ADP
ATP
Newly Synthesized Protein
Translating mRNA
ATP/ADP
ATP/ADP

488

489 **Figure 6:**

490 **Perturbation of AMPK function disrupts receptor specific translation response:**

491 **(A)** Representative images showing phospho-eEF2 immunolabeling (Pseudo-colored) in cortical
492 neurons on basal condition, on DHPG (50μM) treatment for 5 minutes in presence or absence of
493 AICAR (1mM). MAP2B immunolabeling (supplementary figure 5B) was used for identifying
494 neurons and intensity was used for normalization. Scale=10μM.

495 **(B)** Box plot showing phospho-eEF2 intensity distribution across multiple neurons on basal
496 condition, on DHPG treatment for 5 minutes, on AICAR treatment for 1 hour and on DHPG
497 treatment along with AICAR pre-treatment. *$p<0.05$, **$p<0.01$, ****$p<0.0001$, n=17-46 cells per
498 group from 3 independent plating. One-way ANOVA followed by Bonferroni's multiple
499 comparison test.

500 **(C)** Representative images showing newly synthesized proteins visualized through FUNCAT
501 metabolic labeling (pseudo-colored) in cortical neurons under basal condition, on DHPG
502 treatment for 5 minutes in presence or absence of AICAR. MAP2B immunolabeling
503 (supplementary figure 5B) was used for identifying neurons and intensity was used for
504 normalization. Scale=10μM.

505 **(D)** Box plot showing FUNCAT intensity distribution across multiple neurons on basal condition,
506 on DHPG treatment for 5 minutes, on AICAR treatment for 1 hour and on DHPG treatment along
507 with AICAR pre-treatment. ****$p<0.0001$, n=18-57 cells per group from 3 independent plating.
508 Kruskal-Wallis test followed by Dunn's multiple comparison test.

509 **(E)** Representative images showing phospho-eEF2 immunolabeling (Pseudo-colored) in cortical
510 neurons on basal condition, on NMDA (20μM) treatment for 5 minutes in presence or absence of

511 Compound C (10μM). MAP2B immunolabeling (supplementary figure 5B) was used for identifying
512 neurons and intensity was used for normalization. Scale=10μM.

513 **(F)** Box plot showing phospho-eEF2 intensity distribution across multiple neurons on basal
514 condition (Vehicle control), on NMDA treatment for 5 minutes, on Compound C pre-treatment
515 for 1 hour and on NMDA treatment along with Compound C pre-treatment. *$p<0.05$, **$p<0.01$,
516 n=21-36 cells per group from 3 independent plating. Kruskal-Wallis test followed by Dunn's
517 multiple comparison test.

518 **(G)** Representative images showing newly synthesized proteins visualized through FUNCAT
519 metabolic labeling (pseudo-colored) in cortical neurons under basal condition, on NMDA (20μM)
520 treatment for 5 minutes in presence or absence of Compound C (1mM). MAP2B immunolabeling
521 (supplementary figure 5C) was used for identifying neurons and intensity was used for
522 normalization. Scale=10μM.

523 **(H)** Box plot showing FUNCAT intensity distribution across multiple neurons on basal condition,
524 on NMDA treatment for 5 minutes, on Compound C treatment for 1 hour and on NMDA treatment
525 along with Compound C pre-treatment. *$p<0.05$, **$p<0.01$, ****$p<0.0001$, n=24-52 cells per group
526 from 3 independent plating. Kruskal-Wallis test followed by Dunn's multiple comparison test.

527 **(G)** Schematic showing receptor specific regulation of AMPK-eEF2 signaling and their subsequent
528 impact on global translation. mGluR stimulation (Left) have been found to inactivate AMPK
529 necessary for subsequent downregulation of eEF2 phosphorylation. This led to enhanced global
530 *de-novo* translation and consumption of ATP, hence reducing neuronal ATP/ADP ratio. NMDAR
531 stimulation (Right) caused activation of AMPK in extracellular Ca^{2+} dependent manner causing
532 an increase in eEF2 phosphorylation in turn. This leads to inhibition of global translation
533 therefore having no significant alterations in cellular ATP/ADP ratio.

534

535 **Discussion:**

536 In this work we present multiple lines of evidences showing that activity induced protein
537 synthesis contributes significantly to the energy expenditure in neurons on glutamate
538 stimulation. Our work demostrate that the global de-novo protein synthesis is
539 dynamically regulated by mGluRs and NMDARs with distinct kinetics. As a consequence,
540 we also observed dynamic alterations in energy level with charecteristic temporal
541 features specific to each type of stiumulus. An AMPK-eEF2 signaling nexus combines
542 uniquely to bring about the charecteristic changes in translation with distinct
543 mechanisms for each stimulus.

544 **Protein Synthesis is the major energy consumer on glutamate stimualtion**

545 It was predicted that activity dependent ATP consumption in neurons is largely due to
546 the reversal of ionic fluxes [7]. Our study for the first time establishes the significant
547 effect of activity induced protein synthesis on neuronal energy expenditure.
548 Interestingly we failed to observe any noteworthy contribution from vesicle endocytosis
549 at the pan-neuronal ATP level, unlike what has been observed previously in the axon
550 terminals [8]. This demonstrates the distinct nature of energy regulations in various
551 compartments as compared to that of the whole neurons.

552 **mGluRs and NMDARs affect rate of global translation differently**

553 We identified distinct roles for mGluRs and NMDARs in glutamate driven energy usage.
554 Our results demonstrates mGluR dependent translation activation consumes significant
555 amount of ATP and shares distinct kinetic features to that of NMDAR. Gp I mGluRs have
556 been widely reported to activate protein synthesis [3215] and induce or facilitate long-

557 term depression in excitatory synapses [14] across various brain regions [reviewed in
558 [333435]]. Our results indicate that, mGluR mediated translation activation impact global,
559 dendritic and synaptic energy level immediately. Contrarily, NMDAR stimulation
560 accompanies a delayed impact on global, dendritic or synaptic ATP levels through a
561 delayed translation activation as observed previously [16].

562 **The AMPK-eEF2 Signaling to create differential respnse**

563 Our results describe a key role for AMP activated protein Kinase in both mGluR and
564 NMDAR mediated translation regulation. While AMPK is demonstrated to regulate
565 activity induced energy metabolism [17], sustained activity induced GLUT4 membrane
566 expression in nerve terminals [36] and various forms of synaptic plasticity [2122], our study
567 provide mechanistic basis coupling its role on regulation of energy metabolism and
568 translation. AMPK is known to influence eEF2 Kinase function either directly [37] or
569 through indirect mechanisms involving inhibition of mTOR-S6K pathway [38], thereby
570 regulating global translation. mGluR mediated inactivation of AMPK can thus also create
571 opportunity for increased mTOR-S6K activity as observed previously [39]. These results
572 therefore could explain the dephosphorylation of eEF2 downstream of mGluR
573 stimulation, an effect unexplored previously. The fact that mGluR mediated AMPK
574 activation is protein synthesis depndent led to us investigate the role of AMPK specific
575 phosphatase α-SNAP [31] in this scenario. Increased α-SNAP level and its association with
576 AMPK on mGluR stimulation suggestive of a feedback regulation of AMPK function.
577 NMDAR stimulation on the contrary involved Ca^{2+} dependent activation of AMPK
578 probably involving one of its upstream kinase CamKIIß. This coalates well with the

579 enhanced phosphorylation of eEF2 on NMDA treatment (**supplementary figue 4D**) as
580 observed previously [40].

581 The study also clearly demostrates the importance of protein synthesis in neuronal
582 energy budget particularly during neuronal activity. AMPK plays a pivotal role in
583 dictating this corelation. A deeper elucidation of this corelation would be of greater
584 significance in many patho-physiological conditions such as stroke, epilepsy and
585 neurodegenrerative diseases. Unraveling other signaling mechanisms underlying the
586 connection between protein sysnthesis and energy dynamics and their long term effect
587 on synaptic plasticity may also provide potential theraputic targets for diseases
588 involving impairment in energy metabolism and dysregulated protein synthesis.

589 **Materials and Methods**

590 **Ethics Statement:** All animal work was done in compliance with the procedures
591 approved by the Institutional Animal Ethics committee (IAEC) and the Institutional
592 Biosafety Committee (IBSC), InStem, Bangalore, India. All Work was done with Sprague
593 dawley (SD)rats. Rats were kept in 20-22'c temperature, 50-60 relative humidity, 0.3μm
594 HEPA filtered air supply at 15-20 ACPH and 14/10 light/dark cycle maintained. Food
595 and water were provided *ad libitum*.

596 **Antibodies and Drugs:** Anti-phospho eEF2 antibody (Thr 56; cat no: 2331; Used at
597 1:1000 dilution for western blotting analysis and 1:250 for immunocytochemistry), anti-
598 eEF2 antibody (cat. no 2332; Used at 1:1000 dilution for western blotting analysis),
599 Anti-phospho AMPKα antibody (Thr 172; cat. no: 2535; used at 1:500 dilution for western
600 blotting analysis and 1:100 for immunocytochemistry analysis), anti-AMPK antibody (cat

601 no: 2532; used at 1:1000 dilution for western blotting analysis), Anti-phospho ACC
602 antibody (cat no: 3661; used at 1:1000 dilution for western blotting analysis) were
603 obtained from Cell Signalling Technologies (MA, US). Anti- tubulin antibody (cat no:
604 T9026; used at 1:1000 dilution for western blotting analysis), anti-MAP2B antibody (cat
605 no: M9942; used at 1:500 dilution for immunocytochemistry), anti-rabbit HRP labelled
606 secondary antibody (cat no: A0545 ; used at 1:5000 dilution for western blotting
607 analysis), anti-mouse HRP labelled secondary antibody (cat no: A9044 ; used at 1:5000
608 dilution for western blotting analysis) were obtained from Sigma-Aldrich (St. Louis, MO).
609 Anti-rabbit secondary antibody alexa 555 labelled (cat no: A11032; used at 1:500
610 dilution for immunocytochemistry) and anti-mouse secondary antibody alexa 488
611 labeled (cat no: A11008; used at 1:500 dilution for immunocytochemistry) were
612 obtained from Thermo fisher Scientific (Waltham, MA). Anti-α-SNAP antibody (cat no:
613 X1026; used at 1:1000 dilution for western blotting analysis). Glutamate (25μM), NMDA
614 (20μM for neurons and 40μM for SNS), CNQX (40μM), Anisomycin (25μM for neurons and
615 50μM for synaptoneurosomes), Cycloheximide (100μg/ml), Ouabain octahydrate (1mM),
616 Dynasore hydrate (100μM), Poly-L-Lysine (0.2mg/ml), Pluronic-F-127(0.002%), BAPTA
617 (10mM) and Ionomycin (10μM) were obtained from Sigma-aldrich (St. Louis, MO). S-3,5
618 DHPG (20μM for neurons and 100μM for SNS), 5-aminoimidazole-4-carboxamide
619 ribonucleotide (AICAR, 1mM), D-AP5 (25μM), MK-801 (10μM) and mPEP (10μM) were
620 obtained from Tocris Biosciences. Compound C (dorsomorphin; 40μM in
621 synaptoneurosomes and 20μM in cultured neurons) were obtained from Santa Cruz
622 Biotechnology (Santa Cruz, CA). Fuo-8 AM (2μM) was obtained from AAT Bioquest
623 (Sunnyvale, CA).

624 **Synaptoneurosome preparation** Synaptoneurosomes were prepared from SD WT rat
625 cortices at the age between post-natal day 28-33 (P28-33) following differential
626 centrifugation method as described previously (Hollingsworth et al., 1985 Scheetz,
627 Nairn, & Constantine-paton, 2000 R. S. Muddashetty, Kelic, Gross, Xu, & Bassell, 2007).
628 Briefly, rat cortices were dissected and homogenized at 4°C in 8 volumes of
629 synaptoneurosome (SNS) homogenization buffer [containing (in mM) 25 Tris-HCl pH 7.4,
630 118 NaCl, 4.7 KCl, 1.2 MgSO4, 2.5 CaCl2, 1.53 KH2PO4 and 212.7 glucose, ,
631 supplemented with Complete protease inhibitors (Roche)]. Homogenates were then
632 passed through three 100µm nylon mesh filters followed by one 11µm filter MLCWP 047
633 Millipore (Bedford, MA) and centrifuged at 1000g for 20 minutes at 4°C. The pellet was
634 resuspended into 2ml of the same buffer. In experiments with no Ca^{2+}, $CaCal_2$ was not
635 added in the resuspension buffer. The resuspended SNS particles were then incubated
636 at 37°C to make them metabolically active.

637 **Synaptoneurosome Stimulation:** For Stimulation, synaptoneurosomes were pre-
638 warmed at 37°C for minimum of 5 minutes. A sample fraction aliquoted at this point
639 was considered unstimulated condition or 0 min of stimulation for further analysis. This
640 was followed by Gp I mGluR and NMDAR stimulation with specific agonists (s)3,5-
641 dihydroxyphenylglycine (DHPG; 100µM) and N-methyl D-aspartate (NMDA; 40µM)
642 respectively. Further fractions were collected after 2 minutes and 5 minutes of
643 stimulation. A fraction was collected 5 minutes post-stimulation (5 min stimulation + 5
644 min recovery). For this, the synaptoneurosomes were first stimulated for 5 minutes with
645 agonists. This is followed by removal of the stimulus through centrifugation at 13,000g
646 for 20 seconds and resuspension with 37°C pre-warmed synaptoneurosome

647 homogenization buffer. These synaptoneurosomes were further incubated for 5 minutes
648 and processed for ATP measurement, protein estimation and western blot analysis. For
649 ATP measurements, stimulation was terminated by direct lysis of synaptoneurosomes
650 with equal volume of boiling water [43]. This was followed by centrifugation at 20,000g
651 for 2.5 minutes for the measurement of soluble ATP content from the supernatant. For
652 protein estimation and western blot analysis, synaptoneurosomes fractions were
653 centrifuged at 13,000g for 20 seconds followed by lysing with lysis buffer [containing:]
654 (**Stimulation protocol figure 2F**). In experiments involving pre-treatment of drugs, pre-
655 warming period varied depending on the incubation period of various drugs which were
656 directly added after the resuspension step. Untreated control synaptoneurosomes were
657 pre-incubated for same period as drug pre-treatment time for comparisons.

658 **Cell line and primary neuronal culture** Primary neurons were cultured from cerebral
659 cortices as described by Banker & Goslin, 1998. Embryos were obtained from females
660 at the 18th day of gestation period (E18) and cerebral cortices were dissected out in ice
661 cold Hank's balanced salt solution under a dissection microscope. Cells were dissociated
662 with 0.25% trypsin solution at 37°C for 10 minutes followed by mechanical trituration
663 in minimal essential medium (MEM, Thermo fisher) with 10% foetal bovine serum
664 (sigma). Dissociated cells were plated on tissue culture dishes or coverslips coated with
665 poly-L-lysine (0.2 mg/ml in borate buffer, pH 8.5). Neurons were attached to the
666 substrate in MEM with 10% FBS for 3h, followed by defined Neurobasal Medium
667 (Invitrogen) with GlutaMAX™ supplement (Gibco™) and B-27 supplements (Invitrogen)
668 for 14 days at 37°C in a 5% CO_2 environment. For immunocytochemistry, cells plated on
669 coverslips kept in a 10cm diameter tissue culture dish with a plating density of 10^5

670 cells/dish. The coverslips are then inverted onto astroglial bed in neurobasal media
671 after substrate attachment in MEM. For biochemical and immunoblotting experiments,
672 cells were grown on 6 well dishes or 35mm diameter dishes with seeding density
673 $4X10^5$/well. For live imaging experiments, cells were seeded with $2X10^5$/35mm
674 diameter glass bottom dishes.

675 **Metabolic Labelling:** For metabolic labelling of proteins, neurons were incubated for 1
676 hour in methionine-free Dulbecco's Modified Essential Medium (DMEM, Thermo Fisher).
677 This was followed by addition of L-azidohomoalanine (AHA; 1μM) for next 55 minutes in
678 the same medium. At this point a group of cells were fixed with 4% Paraformaldehyde
679 (PFA) for 20 minutes and would be considered as unstimulated basal for further analysis.
680 This was followed by either fixing the cells with 4% PFA or the cells were stimulated
681 with mGluR and NMDAR specific agonists DHPG (50uM) and NMDA (20 uM) respectively
682 for 2 minutes, 5 minutes or post stimulation 5 minutes recovery (5 min stim + 5 min
683 recovery) and subsequently fixed with 4% PFA. Cells were then permeabilized in TBS_{50}
684 [containing (in mM):50 Tris-Base, 150 NaCl] + 0.3% Triton X 100 solution and blocked
685 using TBS_{50} + 0.1% Triton X 100 + 2% BSA + 4% FBS containing blocking solution. Newly
686 synthesized proteins were then labeled with Alexa-Fluor-555–alkyne [Alexa Fluor 488 5-
687 carboxamido-(propargyl), bis (triethylammonium salt)], by allowing the fluorophore
688 alkyne to react with AHA azide group through click chemistry. All reagents were from
689 Thermo Fisher and stoichiometry of reagents were calculated according to the
690 suggested manual by the manufacturer (CLICK-iT cell reaction buffer kit, cat.no.
691 C10269). Signal intensity was then measured using confocal microscopy to calculate the

692 amount of newly synthesized proteins. For specific detection of neuronal cells, MAP2B
693 positive cells were used for analysis.
694 **Immunocytochemistry:** Rat primary cortical neurons were stimulated with either 50μM
695 DHPG or 20μM NMDA for 5mins. Cells were fixed with 4% PFA and processed for imaging
696 as described before. In brief, cells were permeabilized using TBS_{50} + 0.3% T solution and
697 were treated with Tris-Glycine solution (containing in Moles: 0.5 Tris-base and 0.2
698 Glycine) before blocking with blocking buffer [TBS_{50} + 0.1% T) + 2% BSA + 4% FBS].
699 Primary antibodies were incubated in blocking buffer overnight at 4°C under gentle
700 shaking condition followed by washes. Alexa Fluor 488 coupled anti-mouse and Alexa
701 Fluor 555 coupled anti-rabbit secondary antibodies were incubated for 2h at room
702 temperature. Finally, coverslips were mounted for imaging using Mowiol® 4-88
703 mounting media. Images were acquired on a Leica TCS SP5 confocal microscope (Leica
704 Biosystems) with HCX PL APO 63X, NA 1.4, oil immersion objective. Imaging conditions
705 were kept constant across groups. Images were acquired on Olympus FLUOVIEW 3000
706 confocal laser scanning microscope (Olympus Corporation) with HCX PL APO 60x, NA
707 1.4, oil immersion objective. For quantification of fluorescence intensities, images
708 were acquired while keeping the open pinhole configuration to collect lights from
709 planes below and above the focal plane as well. Objective was moved in the Z direction
710 with a step size of 0.5μm for 12 such steps to ensure the light was collected from the
711 entire cell across its thickness. For quantification of colocalization, images were
712 acquired using 2.5x optical zooming of to satisfy Nyquist's sampling theorem of
713 information theory for maximum resolution in the XY direction. Pinhole was kept at 1
714 Airy unit to ensure optimum resolution and confocal stacks were acquired with a step

715 size of 0.3μm calculated based on the fluorophore wavelength. Imaging conditions were
716 kept constant across different data sets, across experiments.

717 **Live Cell fluorescence Microscopy:**

718 **Imaging Dendritic ATP/ADP Ratio:** Cells were imaged on Zeiss LSM 780 confocal laser
719 scanning microscope (Car Zeiss, Oberkochen, Germany) with 63X Zeiss plan-apochromat
720 oil immersion objective, NA 1.4 with argon lasers of specified wavelength. Cells were
721 grown in Neurobasal media containing B27 supplements and Glutamax and were
722 transfected with PercevalHR and pH-Red construct for simultaneous monitoring of
723 intracellular ATP/ADP ratio and pH. pH monitoring was done as suggested in previous
724 studies [45] to correct for the bias created in Perceval HR fluorescence solely due to the
725 change in intracellular pH. Perceval HR was excited with 488/20 nm and 405/20 nm
726 band-pass filters and emission was collected through a 520/15nm band-pass filter.
727 Excitation and emission beams were separated through 490 nm short pass dichroic
728 mirror. pH-Red was excited using 561/20nm and 455/10 nm band-pass filters and
729 emission was collected through 630/50 nm band pass filter. A 560 nm short-pass dichroic
730 was used to separate excitation and emission beams.
731 Neurons were imaged at room temperature in 37°C pre-warmed Neurobasal media
732 without phenol red (Thermo Fisher, Waltham, MA, USA) containing 15mM HEPES. For,
733 approximate pH bias removal, the linear relationship established between Perceval HR
734 and pH-Red fluorescence for the high glucose 'ATP Loaded' state by Tantama et. Al.,
735 2014 was used. The relationship was used to predict the pH bias of Perceval HR signal
736 from the continuously monitored pH-Red signal and was normalized to the observed

737 Perceval HR fluorescence for the entire period of experiment. Images were captured at
738 16-bit image format with 512X512 pixel distribution with frame rate of 1 per 15 seconds.
739
740 **Ca^{2+} Imaging:** Growth media from cells grown on glass bottom petri dishes were first
741 removed and were washed with imaging media [containing in mM: 120 NaCl, 3 KCl, 2
742 CaCl2, 1MgCl2, 3 NaHCO3, 1.25 NaH2PO4, 15 HEPES, 30 glucose (pH 7.4). They were
743 then incubated with 2 ml freshly prepared dye solution (2 μM Fluo-8 AM and 0.002%
744 Pluronic F-127 in imaging media) at 37°C for 10 mins followed by a 5 minutes incubation
745 procedure at the same temperature with the imaging media. They were then imaged
746 on Olympus FV3000 confocal laser scanning inverted microscope with 20X air objective
747 lens NA 0.75, illuminated with 488nm solid state lasers. Images were acquired at a rate
748 of single frame per 3.22 sec intervals at room temperature. Cells were imaged for 322
749 sec (100 frames) for recording spontaneous activity, followed by 644 sec (200 frames)
750 with stimulant and 161 sec (50 frames) with KCl (to check neuronal activity) or
751 ionomycin (F_{max}). After background, fluorescence were calibrated to $[Ca^{2+}]_i$ as $[Ca^{2+}]_i$ =
752 389 $(F-F_{min})/(F_{max}-F)$nM. F_{min} was recorded by chelating Ca^{2+} with 10μM ionomycin
753 (Calbiochem) and 10mM BAPTA (Sigma) in independent experiments and F_{max} was
754 recorded by 10μM ionomycin in presence of 2.5mM $CaCl_2$ in each experiment.

755 **Luciferase Assay:** To measure synaptic ATP levels, Cortical synaptoneurosomes were
756 first pre-warmed and then stimulated with Gp I mGluR and NMDAR specific agonists at
757 37°C under constant shaking. Fractions of the stimulated solutions were collected at
758 time points specified before. For treatment with various drugs, the pre-warming period
759 varied depending on the pre-incubation time of the drug before the stimulants were

760 added. Collected fractions were added to equal volume of boiling water to extract the
761 ATP as described previously (Yang et al., 2002). The lysates were then used for
762 quantification of soluble ATP molecules using luciferase based commercial ATP
763 quantification kit (ATP Determination kit, Thermo fisher, Cat.no. A22066) with the help
764 of a standard curve. For measuring ATP/ADP ratio from cortical neurons, cells were
765 stimulated for specified time points and lysed with lysis buffer [containing in mM: 50
766 Tris-Cl (pH-7.4), 150 NaCl, 5 $MgCl_2$, 1% Triton-X-100, supplemented with EDTA free
767 protease inhibitor complex (Sigma, cat. no. S8830) and phosphatase inhibitor cocktail
768 (Roche, ref.no. 04906837001)]. Lysates were then centrifuged at 20,000g for 20 minutes
769 and supernatants were used for measuring ATP using luciferase-based protocol. This
770 was followed by a step converting ADP to ATP which was then used to measure the ATP
771 and ADP level together constituting majority of the adenine nucleotides. This was done
772 using a commercially available luminescence-based kit (ADP/ATP ratio kit, Abcam,
773 cat.no. ab65313) following the user manual suggested by the manufacturer.

774 **Image Analysis:** Image analysis was done using Fiji (ImageJ based image processing
775 package) and IMARIS 9.0 (Bitplane, Oxford instrument company, Belfast, UK) software.
776 For fluorescence intensity quantification, confocal stacks were collapsed using sum
777 slice projection method and mean intensity was quantified from the cells. MAP2B
778 positive cells were used for identification of neurons and quantified mean intensity
779 values were used for normalization. For quantifying co-localization, Pearson's
780 correlation coefficient (PCC) was measured for the cell body and proximal dendrite
781 region (<50μm). For the coefficient analysis, measurement was done after manual
782 thresholding with threshold value of 155 for a 12bit image format. For time frame

783 analysis, mean fluorescence intensity was quantified for the imaged dendritic region
784 from each time frame. Time frame analysis was done using the time series analyser V3
785 plug in from Fiji. Representative images for ratiometric quantifications were generated
786 using the Ratio Plus plug from Fiji where the image was generated by calculating pixel
787 by pixel intensity ratio between two channels.

788 **Statistical Analysis:** Statistical comparisons were done using GraphPad Prism (Prism
789 7.01, Graphpad Software Inc, La Jolla, CA, USA). For group comparisons, the data
790 distributions were first tested for normality using Kolmogorov-Smirnov Goodness-of-Fit
791 Test or Shapiro-Wilk normality test. Depending on the distribution, either parametric
792 or non-parametric tests were used to quantify statistical significance. For groups with
793 <4 data points, the inherent distribution was considered to follow Gaussian distribution
794 unless mentioned. For comparing two groups, Student's t test (two tailed,
795 paired/unpaired) was done to calculate statistical significance. Multiple group
796 comparisons were made using one-way ANOVA followed by Bonferroni's multiple
797 comparison test for parametric distribution and Kruskal-Wallis's Test followed by
798 Dunn's Multiple comparison test. Two-way ANOVA followed by Holm Sidak's multiple
799 comparison test was performed for comapring multiple groups at various time points.
800 Data are presented as mean ± SEM. p values < 0.05 was considered statistically
801 significant.

802 **Acknowledgement**

803 We are thankful to Central Imaging and Flow-cytometry Facility (CIFF) for LSM 780 and
804 FV3000 confocal microscopes, NCBS animal house facility for generously maintingng the
805 rat colony needed for experimentation. We extend our gratitude to Professor M.K.

806 Mathew and Dr. Tina Mukherjee for their helpful comments and discussion. We thanks
807 Chaitra Ananda, Amirthavarshini Devrajan and Sonu. P. Kurien for their gracious efforts
808 in experimental support and data analysis. The work was supported by the Neurostem
809 grant (BT/IN/Denmark/07/RSM/2015-2016) and Center for Brain Development and
810 Repair (CBDR) (BT/MB-CNDS/2013), Department of Biotechnology, Govt. of India. We
811 thank Dr. Garry Yellen, Harvard University for his useful suggestions on PercevalHR
812 experiments.

813 **Author contribution**

814 S.G.D designed and performed the experiments, analyzed data and co-wrote the
815 manuscript. Sumita.C performed Calcium imaging experiments and analyzed data,
816 Sumantra C. provided resources, A.B provided resources and analyzed data, R.M
817 designed experiments and co-wrote manuscripts.

818 **References**

819 1. Mink, J. W., Blumenschine, R. J. & Adams, D. B. Ratio of central nervous system
820 to body metabolism in vertebrates: its constancy and functional basis. *Am. J.*
821 *Physiol. Integr. Comp. Physiol.* **241,** R203–R212 (1981).

822 2. Rooijackers, H. M. M., Wiegers, E. C., Tack, C. J., Van Der Graaf, M. & De
823 Galan, B. E. Brain glucose metabolism during hypoglycemia in type 1 diabetes:
824 Insights from functional and metabolic neuroimaging studies. *Cell. Mol. Life Sci.*
825 **73,** 705–722 (2016).

826 3. Schurr, A. Lactate, glucose and energy metabolism in the ischemic brain
827 (Review). *Int. J. Mol. Med.* **10,** 131–136 (2002).

828 4. Koenig, J. B. & Dulla, C. G. Dysregulated Glucose Metabolism as a Therapeutic
829 Target to Reduce Post-traumatic Epilepsy. *Front. Cell. Neurosci.* **12,** 350
830 (2018).

831 5. Vallée, A., Lecarpentier, Y., Guillevin, R. & Vallée, J. N. Demyelination in
832 multiple sclerosis: Reprogramming energy metabolism and potential PPARγ
833 agonist treatment approaches. *Int. J. Mol. Sci.* **19,** (2018).

834 6. Attwell, D. & Laughlin, S. B. An energy budget for signaling in the grey matter
835 of the brain. *J. Cereb. Blood Flow Metab.* **21,** 1133–1145 (2001).

836 7. Harris, J. J., Jolivet, R. & Attwell, D. Synaptic Energy Use and Supply. *Neuron*
837 **75,** 762–777 (2012).

838 8. Rangaraju, V., Calloway, N. & Ryan, T. A. Activity-driven local ATP synthesis is
839 required for synaptic function. *Cell* **156,** 825–835 (2014).

840 9. Pathak, D. *et al.* The role of mitochondrially derived ATP in synaptic vesicle
841 recycling. *J. Biol. Chem.* **290,** 22325–22336 (2015).

842 10. Rangaraju, V., tom Dieck, S. & Schuman, E. M. Local translation in neuronal
843 compartments: how local is local? *EMBO Rep.* **18,** 693–711 (2017).

844 11. Schwanhüusser, B. *et al.* Global quantification of mammalian gene expression
845 control. *Nature* **473,** 337–342 (2011).

846 12. Hunt, D. L. & Castillo, P. E. Synaptic plasticity of NMDA receptors: Mechanisms
847 and functional implications. *Curr. Opin. Neurobiol.* **22,** 496–508 (2012).

848 13. Malenka, L. NMDA Receptor-Dependent Long-Term Potentiation and Long-Term

849 Depression (LTP/LTD). 1–16 (2012). doi:10.1101/cshperspect.a005710

850 14. Huber, K. M., Kayser, M. S. & Bear, M. F. Role for Rapid Dendritic Protein
851 Synthesis in Hippocampal Depression. *Science (80-.).* **288,** 1254–1256 (2000).

852 15. Luchelli, L., Thomas, M. G. & Boccaccio, G. L. Synaptic control of mRNA
853 translation by reversible assembly of XRN1 bodies. *J. Cell Sci.* **128,** 1542–1554
854 (2015).

855 16. Scheetz, A. J., Nairn, A. C. & Constantine-paton, M. NMDA receptor-mediated
856 control of. 211–216 (2000).

857 17. Marinangeli, C. *et al.* AMP-Activated Protein Kinase Is Essential for the
858 Maintenance of Energy Levels during Synaptic Activation. *iScience* **9,** 1–13
859 (2018).

860 18. Manlio Díaz-García, C. *et al.* Neuronal Stimulation Triggers Neuronal Glycolysis
861 and Not Lactate Uptake Cell Metabolism Article Neuronal Stimulation Triggers
862 Neuronal Glycolysis and Not Lactate Uptake. *Cell Metab.* **26,** 361–374.e4 (2017).

863 19. Rangaraju, V., Lauterbach, M. & Schuman, E. M. Spatially Stable Mitochondrial
864 Compartments Fuel Local Translation during Plasticity. *Cell* **176,** 73–84.e15
865 (2019).

866 20. Burkewitz, K., Zhang, Y. & Mair, W. B. AMPK at the nexus of energetics and
867 aging. *Cell Metab.* **20,** 10–25 (2014).

868 21. Potter, W. B. *et al.* Metabolic regulation of neuronal plasticity by the energy
869 sensor AMPK. *PLoS One* **5,** (2010).

870 22. Kong, D. *et al*. A Postsynaptic AMPK→p21-Activated Kinase Pathway Drives
871 Fasting-Induced Synaptic Plasticity in AgRP Neurons. *Neuron* **91,** 25–33 (2016).

872 23. Tantama, M., Martínez-François, J. R., Mongeon, R. & Yellen, G. Imaging energy
873 status in live cells with a fluorescent biosensor of the intracellular ATP-to-ADP
874 ratio. *Nat. Commun.* **4,** (2013).

875 24. Pedersen, S. F., Jørgensen, N. K., Damgaard, I., Schousboe, A. & Hoffmann, E.
876 K. Mechanisms of pH(i) regulation studied in individual neurons cultured from
877 mouse cerebral cortex. *J. Neurosci. Res.* **51,** 431–441 (1998).

878 25. Dieterich, D. C. *et al*. In situ visualization and dynamics of newly synthesized
879 proteins in rat hippocampal neurons. *Nat. Neurosci.* **13,** 897–905 (2010).

880 26. Sutton, M. A., Taylor, A. M., Ito, H. T., Pham, A. & Schuman, E. M. Postsynaptic
881 Decoding of Neural Activity: eEF2 as a Biochemical Sensor Coupling Miniature
882 Synaptic Transmission to Local Protein Synthesis. *Neuron* **55,** 648–661 (2007).

883 27. Takei, N. *et al*. Brain-derived neurotrophic factor enhances the basal rate of
884 protein synthesis by increasing active eukaryotic elongation factor 2 levels and
885 promoting translation elongation in cortical neurons. *J. Biol. Chem.* **284,** 26340–
886 26348 (2009).

887 28. Richter, J. D. & Coller, J. Pausing on Polyribosomes: Make Way for Elongation in
888 Translational Control. *Cell* **163,** 292–300 (2015).

889 29. Ryazanov, A. G. & Davydova, E. K. Mechanism of elongation factor 2 (EF-2)
890 inactivation upon phosphorylation Phosphorylated EF-2 is unable to catalyze

891 translocation. *FEBS Lett*. **251,** 187–190 (1989).

892 30. Hawley, S. A. *et al*. Characterization of the AMP-activated protein kinase kinase
893 from rat liver and identification of threonine 172 as the major site at which it
894 phosphorylates AMP-activated protein kinase. *J. Biol. Chem*. **271,** 27879–27887
895 (1996).

896 31. Wang, L. & Brautigan, D. L. α-SNAP inhibits AMPK signaling to reduce
897 mitochondrial biogenesis and dephosphorylates Thr172 in AMPKα in vitro. *Nat*.
898 *Commun*. **4,** 1559 (2013).

899 32. Weiler, I. J. *et al*. Fragile X mental retardation protein is necessary for
900 neurotransmitter-activated protein translation at synapses. *Proc. Natl. Acad.*
901 *Sci. USA* **101,** 17504–9 (2004).

902 33. Bellone, C., Lüscher, C. & Mameli, M. Mechanisms of synaptic depression
903 triggered by metabotropic glutamate receptors. *Cell. Mol. Life Sci*. **65,** 2913–
904 2923 (2008).

905 34. Schulte, G. The Class Frizzled Receptors. *Pharmacol. Rev*. **62,** 632–667 (2010).

906 35. Jörntell, H. & Hansel, C. Synaptic Memories Upside Down: Bidirectional
907 Plasticity at Cerebellar Parallel Fiber-Purkinje Cell Synapses. *Neuron* **52,** 227–
908 238 (2006).

909 36. Ashrafi, G., Wu, Z., Farrell, R. J. & Ryan, T. A. GLUT4 Mobilization Supports
910 Energetic Demands of Active Synapses. *Neuron* **93,** 606–615.e3 (2017).

911 37. Browne, G. J., Finn, S. G. & Proud, C. G. Stimulation of the AMP-activated

912 Protein Kinase Leads to Activation of Eukaryotic Elongation Factor 2 Kinase and
913 to Its Phosphorylation at a Novel Site, Serine 398. *J. Biol. Chem.* **279,** 12220–
914 12231 (2004).

915 38. Inoki, K., Zhu, T. & Guan, K.-L. TSC2 Mediates Cellular Energy Response to
916 Control Cell Growth and Survival phosphorylation decreases the ability of TSC2
917 to inhibit the phosphorylation of ribosomal S6 kinase (S6K) and eukaryotic
918 initiation factor 4E binding protein-1 (4EBP1). *Cell* **115,** 577–590 (2003).

919 39. Hou, L. Activation of the Phosphoinositide 3-Kinase-Akt-Mammalian Target of
920 Rapamycin Signaling Pathway Is Required for Metabotropic Glutamate Receptor-
921 Dependent Long-Term Depression. *J. Neurosci.* **24,** 6352–6361 (2004).

922 40. Maus, M. *et al.* 2-Deoxyglucose and NMDA inhibit protein synthesis in neurons
923 and regulate phosphorylation of elongation factor-2 by distinct mechanisms. *J.*
924 *Neurochem.* **96,** 815–824 (2006).

925 41. Hollingsworth, E. B. *et al.* Biochemical characterization of a filtered
926 synaptoneurosome preparation from guinea pig cerebral cortex: cyclic
927 adenosine 3':5'-monophosphate-generating systems, receptors, and enzymes. *J.*
928 *Neurosci.* **5,** 2240–2253 (1985).

929 42. Muddashetty, R. S., Kelic, S., Gross, C., Xu, M. & Bassell, G. J. Dysregulated
930 Metabotropic Glutamate Receptor-Dependent Translation of AMPA Receptor and
931 Postsynaptic Density-95 mRNAs at Synapses in a Mouse Model of Fragile X
932 Syndrome. *J. Neurosci.* **27,** 5338–5348 (2007).

933 43. Yang, N. C., Ho, W. M., Chen, Y. H. & Hu, M. L. A convenient one-step

934 extraction of cellular ATP using boiling water for the luciferin-luciferase assay
935 of ATP. *Anal. Biochem.* **306,** 323–327 (2002).

936 44. Banker, G. & Goslin, K. Culturing nerve cells. in *Cellular and molecular*
937 *neuroscience series* **2nd Ed., M,** 666 (1998).

938 45. Tantama, M. & Yellen, G. *Imaging changes in the cytosolic ATP-to-ADP ratio.*
939 *Methods in Enzymology* **547,** (Elsevier Inc., 2014).

940

941

942

943 **Supplementary Information**

944 **Supplementary Figure 1:**

945 **Quantifying Activity dependent changes in energy level.** (Related to Figure 1)

946 **(A)** Bar graph representing normalized average value of neuronal ATP/ATP+ADP ratio in basal
947 condition and on DHPG (50μM) and NMDA (20μM) treatment for 5 minutes. *$p<0.05$, n=3
948 independent plating. One-way ANOVA followed by Bonferroni's multiple comparison test.

949 **(B)** Bar graph representing normalized average value of neuronal ATP/ATP+ADP ratio in basal
950 condition, on dynasore (100μM) treatment for 30 minutes, on Glutamate (25μM) treatment for
951 5 minutes and on glutamate treatment along with dynaosre pre-treatment. *$p<0.05$, n=3-6
952 independent plating. One-way ANOVA followed by Bonferroni's multiple comparison test.

953 **(C)** Quantification showing the effect of treatment of anisomycin, cycloheximide and MPEP on
954 synaptic ATP level measured from cortical synaptoneurosomes. Data = mean ± SEM with
955 scattered data points.

956 **Supplementary Figure 2:**

957 **Sensor Calibration and Basal ATP measurement.** (Related to Figure 2)

958 **(A)** Graph depicting a linear relationship was established between the percevalHR fluorescence
959 ratio and the pH-Red fluorescence ratio using NH_4Cl pre-pulse method following method
960 established previously (Pederson et. al, 1998, Tantama et. al, 2013). Briefly a gradient of 5-
961 15mM NH_4Cl solution was applied to allow the changes in intracellular pH in a short period of
962 time to avoid any metabolic stress. Changes in PercevalHR fluorescence was measured along
963 with pH-Red fluorescence and the linear relation was used to remove pH bias approximately.

964 **(B)** Representative dendrite showing the temporal profile of PercevalHR fluorescence
965 (ATP/ADP) in unstimulated condition. Scale=10μM.

966 **(C)** Average time traces showing the change in the dendritic ATP/ADP ratio on unstimulated
967 condition in presence or absence of anisomycin. Data= mean ± SEM. n≥3 cells from independent
968 platings per group.

969 **(D)** Quantification showing the changes in synaptic ATP level on unstimulated conditions. Data=
970 mean ± SEM. n= 4 animals.

971 **Supplementary Figure 3:**

972 **Translation Kinetics.** (Related to Figure 3)

973 **(A)** Representative images showing newly synthesized proteins visualized through FUNCAT
974 metabolic labeling (pseudo-colored) in cortical neurons at various time points in unstimulated
975 condition. Absence of AHA while metabolic labeling was used as a negative control. MAP2B

976 immunolabeling (green, inset) was used for identifying neurons and intensity was used for
977 normalization. The average trace quantification and data point distribution for unstimulated
978 cells have been presented in Figure 3C and 3D. Scale=10μM.

979 **(B)** Representative images showing immunolabeling of MAP2B (green) in cortical neurons at
980 various time points following DHPG and NMDA treatment for the cells used for FUNCAT intensity
981 quantification. Scale=10μM.

982 **(C)** Representative images showing immunolabeling of MAP2B (green) in cortical neurons in
983 basal condition and DHPG and NMDA treatment for 5 minutes for the cells used for p-eEF2
984 quantification. Scale=10μM.

985 **(D)** Representative immunoblots describing changes in phospho-eEF2 and total-eEF2 levels at
986 various time points after DHPG (50μM) and NMDA (20μM) treatment to cultured cortical neurons.
987 Note in each case phospho and total eEF2 levels were normalized individually to tubulin before
988 calculating the ratio.

989 **(E)** Line graph showing average value for neuronal phospho/total ratio of eEF2 at various time
990 points after DHPG and NMDA treatment and 5 minutes and 10 minutes after recovery. Data:
991 mean +/- SEM, *$p<0.05$, **$p<0.01$, ***$p<0.001$, n= 3 animals per group. Two Way ANOVA followed
992 by Bonferroni's multiple comparison test.

993 **Supplementary Figure 4:**

994 **Baseline eEF2 phosphorylation and Characterization of NMDAR dependent Ca^{2+} entry.**
995 (Related to Figure 4 and Figure 5)

996 **(A)** Representative images showing immunolabeling of MAP2B (green) in cortical neurons in
997 basal condition and DHPG and NMDA treatment for 5 minutes for the cells used for p-AMPK
998 quantification. Scale=10μM.

999 (B) Line graph showing average value for synaptic phospho/total ratio of eEF2 and AMPK at
1000 various time points after DHPG and NMDA treatment and 5 minutes after recovery in cortical
1001 synaptoneurosomes. Data: mean +/- SEM, n≥ 2 animals per group. Two Way ANOVA followed by
1002 Bonferroni's multiple comparison test.

1003 **(C)** Representative images depicting intracellular Ca^{2+} levels (Pseudo-colored) of a cortical
1004 neuron before stimulation, immediately (15s) after NMDA (20μM) treatment, at a later time
1005 point (300sec) after NMDA treatment and after ionomycin treatment along with 10mM Ca^{2+} in
1006 presence MK-801. Scale=20μM.

1007 **(D)** Representative immunoblots describing changes in phospho-eEF2 and total-eEF2 levels at
1008 various time points after NMDA (40μM) treatment to cortical synaptoneurosomes in presence or
1009 absence of extracellular Ca^{2+}. Note in each case phospho and total AMPK levels were normalized
1010 individually to tubulin before calculating the ratio.

1011 **(E)** Line graph showing average value for synaptic phospho/total ratio of eEF2 at various time
1012 points after NMDA treatment and 5 minutes after recovery in presence or absence of Ca^{2+}. Data:
1013 mean +/- SEM, *p<0.05, **p<0.01, n≥ 4 animals per group. Two Way ANOVA followed by
1014 Bonferroni's multiple comparison test.

1015 **Supplementary Figure 5:**

1016 **AMPK perturbations: (related to figure 6)**

1017 **(A)** Representative images showing phospho-eEF2 immunolabeling (Pseudo-colored), newly
1018 synthesized protein through FUNCAT metabolic labeling and MAP2B immunolabeling in cortical
1019 neurons on AICAR (1mM) treatment and Compound C (10μM) treatment for 1 hour. MAP2B
1020 immunolabeling was used for identifying neurons and intensity was used for normalization.
1021 Scale=10μM.

1022 **(B)** Representative images showing immunolabeling of MAP2B (green) in cortical neurons in
1023 basal condition and on DHPG treatment for 5 minutes in presence or absence of AICAR for the
1024 cells used for p-eEF2 and FUNCAT quantification. Scale=10μM.

1025 **(C)** Representative images showing immunolabeling of MAP2B (green) in cortical neurons in
1026 basal condition and on NMDA treatment for 5 minutes in presence or absence of Compound C
1027 for the cells used for p-eEF2 and FUNCAT quantification. Scale=10μM.

1028